A *Plasmodium falciparum* MORC protein complex modulates epigenetic control of gene expression through interaction with heterochromatin

Maneesh Kumar Singh[1#], Victoria A. Bonnell[2,3,4#], Israel Tojal Da Silva[5], Verônica Feijoli Santiago[6], Miriam S. Moraes[1], Jack Adderley[7], Christian Doerig[7], Giuseppe Palmisano[6], Manuel Llinás[2,3,4,8], and Célia R. S. Garcia[1]*

[1] Department of Clinical and Toxicological Analyses, School of Pharmaceutical Sciences, University of São Paulo, São Paulo, Brazil

[2] Department of Biochemistry and Molecular Biology, Pennsylvania State University, University Park, Pennsylvania, United States

[3] Huck Institutes Center for Eukaryotic Gene Regulation, Pennsylvania State University, University Park, Pennsylvania, United States

[4] Huck Institutes Center for Malaria Research, Pennsylvania State University, University Park, Pennsylvania, United States

[5] Hospital AC Camargo, Centro Internacional de Pesquisa, São Paulo, Brazil

[6] Department of Parasitology, Institute of Biomedical Science, University of São Paulo, São Paulo, Brazil

[7] School of Health and Biomedical Sciences, RMIT University, Bundoora, Melbourne, VIC 3083, Australia

[8] Department of Chemistry, Pennsylvania State University, University Park, Pennsylvania, United States

 # coauthorship

*** Corresponding author**

Abstract

Dynamic control of gene expression is critical for blood stage development of malaria parasites. Here, we used multi-omic analyses to investigate transcriptional regulation by the chromatin-associated microrchidia protein, MORC, during asexual blood stage development of the human malaria parasite *Plasmodium falciparum*. We show that *Pf*MORC (PF3D7_1468100) interacts with a suite of nuclear proteins, including APETALA2 (AP2) transcription factors (*Pf*AP2-G5, *Pf*AP2-O5, *Pf*AP2-I, PF3D7_0420300, PF3D7_0613800, PF3D7_1107800, and PF3D7_1239200), a DNA helicase DS60 (PF3D7_1227100), and other chromatin remodelers (*Pf*CHD1 and *Pf*EELM2). Transcriptomic analysis of *Pf*MORC$^{HA\text{-}glmS}$ knockdown parasites revealed 163 differentially expressed genes belonging to hypervariable multigene families, along with upregulation of genes mostly involved in host cell invasion. *In vivo* genome-wide chromatin occupancy analysis during both trophozoite and schizont stages of development demonstrates that *Pf*MORC is recruited to repressed, multigene families, including the *var* genes in subtelomeric chromosomal regions. Collectively, we find that *Pf*MORC is found in chromatin complexes that play a role in the epigenetic control of asexual blood stage transcriptional regulation and chromatin organization.

41 # Introduction

42 Despite global efforts to combat malaria, the disease caused an estimated 249 million new cases
43 and more than 608,000 deaths in 2022 (World Malaria Report 2023). The etiological agents of
44 human malaria are apicomplexan parasites of the genus *Plasmodium*. Among the six known
45 *Plasmodium* species that can infect humans, *Plasmodium falciparum* is the most lethal, causing
46 the majority of annual deaths (Cowman *et al.* 2012). The intraerythrocytic developmental cycle
47 (IDC) of *P. falciparum* is responsible for the clinical symptoms of malaria. The IDC
48 commences when merozoites generated during the liver-stage enter the circulatory system and
49 invade red blood cells (RBCs). While growing inside RBCs, parasites undergo multiple
50 developmental phases with distinct morphological characteristics (ring, trophozoite, and
51 schizont). Maturation and schizogony leads to the formation of 16-32 daughter merozoites
52 destined to invade new RBCs (Singh *et al.* 2010). A small fraction (<10%) of parasites
53 differentiate into non-replicative sexual gametocytes, which are transmitted to the mosquito
54 during a second blood meal to complete sexual development.

55 Parasite development through the asexual blood stage is facilitated by precise transcriptional
56 regulation, where genes are only expressed when needed in a just-in-time fashion (Bozdech *et*
57 *al.* 2003). Approximately 90% of genes across the *P. falciparum* genome are transcribed during
58 the asexual blood stage in a cascade of gene expression believed to be controlled by both
59 sequence-specific transcription factors and dynamic epigenetic changes to chromatin (Painter
60 *et al.* 2011, Toenhake *et al.* 2018, Jeninga *et al.* 2019, Hollin *et al.* 2021). The gene regulatory
61 toolbox in malaria parasites is lacking many transcriptional regulatory factors conserved in
62 other eukaryotes (Gardner *et al.* 2002). The identification of a large family of *Plasmodium*
63 homologues of the plant APETALA2/Ethylene Response Factor (AP2/ERF) transcription
64 factors (TFs) provided a breakthrough to unravel key regulators of gene expression in these
65 parasites (Balaji *et al.* 2005). There are 28 putative APETALA2 (ApiAP2) TFs identified in *P.*
66 *falciparum,* each protein containing one to three AP2 DNA binding domains (Painter *et al.*
67 2011, Jeninga *et al.* 2019). Multiple studies in *Plasmodium spp.,* using a variety of approaches,
68 have characterized essential functions of ApiAP2 TFs in RBC invasion, gametocytogenesis,
69 oocyst formation and sporozoite formation (Yuda *et al.* 2009, Kafsack *et al.* 2014, Sinha *et al.*
70 2014, Modrzynska *et al.* 2017, Santos *et al.* 2017, Zhang *et al.* 2018). ApiAP2 proteins in
71 *Plasmodium* species display a wide array of functions during parasite development in both the
72 vertebrate host and the mosquito vector, but surprisingly, over 70% of ApiAP2 proteins are
73 expressed in the asexual blood stage of the lifecycle (Bozdech *et al.* 2003, Le Roch *et al.* 2003,
74 Chappell *et al.* 2020).

Despite increasing evidence detailing ApiAP2 protein regulatory complexes (Santos *et al.* 2017, Harris *et al.* 2019, Hillier *et al.* 2019, Hoeijmakers *et al.* 2019, Farhat *et al.* 2020, Josling *et al.* 2020, Miao *et al.* 2021, Srivastava *et al.* 2023, Yuda *et al.* 2023, Antunes *et al.* 2024), the functional properties and specific interaction partners of many ApiAP2 TFs remain to be elucidated. A quantitative mass spectrometry-based analysis of the parasite protein interaction network has revealed links between ApiAP2 TFs and many chromatin remodelers, such as an extended Egl-27 and MTA1 homology 2 (EELM2) domain-containing proteins (PF3D7_0519800 and PF3D7_1141800), histone deacetylase protein 1 (HDAC1; PF3D7_0925700), and the microrchidia family protein *Pf*MORC (PF3D7_1468100) (Hillier *et al.* 2019). Genome-wide mutagenesis studies revealed that several genes within these proposed networks, including *pfmorc*, are essential for parasite proliferation (Bushell *et al.* 2017, Zhang *et al.* 2018). Using a targeted deletion strategy, we previously were unable to delete *pfmorc,* further suggesting that it is essential for parasite growth (Singh *et al.* 2021). Moreover, STRING network analysis has shown that the putative ApiAP2:*Pf*MORC complex forms a network with proteins having DNA-binding or nucleosome assembly properties, suggesting that *Pf*MORC may function as an accessory protein in epigenetic regulation (Hillier *et al.* 2019). Previous work identified *Pf*MORC in a chromatin complex containing the chromatin remodeling protein *Pf*ISWI (PF3D7_0624600) located at *var* gene promoter regions (Bryant *et al.* 2020). All *P. falciparum* strains encode roughly 60 highly polymorphic *var* genes, but through an epigenetic allelic exclusion mechanism, each parasite is thought to expresses a single allele (Real *et al.* 2022, Schneider *et al.* 2023). Bryant *et al.* have proposed that *Pf*MORC is recruited to these heterochromatic regions to assist in the silencing of *var* genes, on the basis of its known function as a repressor complex component in model eukaryotes. In the related apicomplexan parasite *Toxoplasma gondii*, *Tg*MORC functions as a repressor of sex-associated genes by recruiting the *Tg*HDAC3 histone deacetylase and forming heterogenous complexes with eleven ApiAP2 TFs (Farhat *et al.* 2020). To date, only two *Tg*MORC:HDAC3 complexes have been characterized, including a dimeric *Tg*AP2XII-2:HDAC3 complex and a heterotrimeric *Tg*AP2XII-1:AP2XI-2:HDAC3 complex (Srivastava *et al.* 2023, Antunes *et al.* 2024).

MORC proteins canonically consist of two major conserved regions: (1) a catalytic ATPase domain at the N-terminus (comprising a GHKL [Gyrase, HSP90, Histidine kinase, and MutL] domain and S5 fold domain) and (2) a C-terminal protein-protein interaction domain containing one or more coiled-coils (Koch *et al.* 2017). The conserved MORC gene family is present in most eukaryotes (with the exception of fungi), often with multiple paralogs per genome (Dong *et al.* 2018), and has been extensively investigated in various model systems in the context of

109 epigenetic gene regulation. In plants, MORC proteins function in gene repression and
110 heterochromatin compaction (Koch *et al.* 2017, Zhong *et al.* 2023). Additionally, MORC
111 proteins have been shown to play diverse roles in metazoans by forming protein-protein
112 interactions with immune-responsive proteins, SWI chromatin remodeling complexes, histone
113 deacetylases, and histone tail modifications (Iyer *et al.* 2008, Kang *et al.* 2012, Moissiard *et al.*
114 2012, Bordiya *et al.* 2016, Kim *et al.* 2019).
115 While most metazoans possess five to seven MORC paralogs, apicomplexan parasites contain
116 a single *morc* gene (Iyer *et al.* 2008), which encodes not only the canonical animal-like GHKL
117 ATPase domain, but also three Kelch-repeats, and a CW-type zinc-finger domain not found in
118 mammalian MORCs (Farhat *et al.* 2020). This unique domain architecture suggests that the
119 apicomplexan MORC proteins may have parasite-specific roles. To dissect the functional roles
120 of *Pf*MORC, we conducted a proteomic analysis with *Pf*MORC^{GFP}, which identified several
121 nuclear proteins, including a cluster of ApiAP2 TFs, as possible interacting partners. We also
122 determined the genome-wide localization of *Pf*MORC at multiple developmental stages, which
123 revealed *Pf*MORC recruitment predominantly to subtelomeric regions, corroborating that
124 *Pf*MORC may act as a repressor of the clonally variant gene families that are important
125 contributors to malaria pathogenesis. Finally, we performed transcriptomic analysis in
126 *Pf*MORC$^{HA\text{-}glmS}$ knockdown parasites at the asexual stage to investigate alterations in global
127 gene expression. We observed an overrepresentation of downregulated genes belonging to the
128 heterochromatin-associated hypervariable gene family proteins. Overall, this study allows us to
129 assign a role for *Pf*MORC in facilitating the plasticity of epigenetic regulation during asexual
130 blood stage development.
131

132 # Results

133 ***Proteins that co-purify with PMORC represent gene regulatory and chromatin remodeling***
134 ***components***

135 A previous study using Blue-Native PAGE identified a *Pf*MORC complex in association with
136 ApiAP2 proteins and chromatin remodeling machinery (Hillier *et al.* 2019). To validate this
137 observation and expand the repertoire of *Pf*MORC interactors, we used a targeted
138 immunoprecipitation approach coupled to LC–MS/MS proteomic quantification. We used a
139 previously generated *Pf*MORC^{GFP} parasite line (Singh *et al.* 2021) to carry out
140 immunoprecipitation with an anti-GFP antibody at the trophozoite stage, where *Pf*MORC is
141 abundant (Singh *et al*. 2021). The *P. falciparum* 3D7 strain expressing wild-type *pfmorc* was used

142 as a negative control. Trophozoite lysates were incubated with anti-GFP-Trap-A beads
143 (ChromoTek, gta-20), and the immunocaptured proteins were resolved by SDS–PAGE
144 (**Supplemental Figure 1A**). We applied a label-free quantitative proteomics approach with a
145 false discovery rate (FDR) of 1% and number of peptides ≥2 to excised gel samples to identify
146 proteins interacting with *Pf*MORC^{GFP}. From three biological replicates, we identified 211, 617,
147 and 656 proteins respectively. We further identified the overlap between all three wild-type 3D7
148 and *Pf*MORC^{GFP} replicates and found a total of 132 and 142 proteins, respectively
149 (**Supplemental Figure 1B-D, Supplemental Table 1**).
150 To analyze the relative ratio of proteins between wild-type 3D7 and *Pf*MORC^{GFP} groups, we used
151 the mean-normalized MS/MS count to calculate a fold change from *Pf*MORC^{GFP}/3D7, and
152 selected differentially abundant proteins above a 1.5x cutoff filter. This high stringency threshold
153 was used to preclude any mis-identification of *Pf*MORC interactors caused by variability between
154 the replicates **(Figure 1A, Supplemental Figure 1D)**. This analysis resulted in 143 significantly
155 enriched proteins (**Supplemental Table 2**). From these candidate PfMORC-interacting proteins,
156 the top enriched protein (20.8-fold enrichment) was *Pf*EELM2 (PF3D7_0519800, -*log10 p-value*
157 3.43). *Pf*EELM2 was previously predicted as a *Pf*MORC interactor (Hillier *et al.* 2019) and
158 identified in a quantitative histone peptide pulldown to be consistently recruited to
159 H2B.Z_K13/14/18a (Hoeijmakers *et al.* 2019). Similarly, EELM2 of the related Apicomplexan
160 parasite *T. gondii* was recently identified in a *Tg*MORC-associated complex (Farhat *et al.* 2020).
161 We also detected numerous ApiAP2 transcription factors [*Pf*AP2-G5, *Pf*AP2-O5, *Pf*AP2-I,
162 PF3D7_1107800, PF3D7_0613800, PF3D7_0420300 and PF3D7_1239200] (**Table 1**), similar
163 to results reported both by Hillier et al. (Hillier *et al.* 2019) and in the *Toxoplasma* studies which
164 also predicted or experimentally identified many ApiAP2 interactions (Farhat *et al.* 2020,
165 Srivastava *et al.* 2023, Antunes *et al.* 2024). *Pf*AP2-G5 (PF3D7_1139300, -*log10 p-value* 0.22)
166 and *Pf*AP2-O5 (PF3D7_1449500, -*log10 p-value* 0.41) were enriched 20.5-fold and 14.99-fold,
167 respectively, suggesting that these factors are likely major components in complex with
168 *Pf*MORC. To corroborate our results, we compared our *Pf*MORC^{GFP} coIPed proteins to a recently
169 published, computationally predicted, protein–protein interaction network (Hillier *et al.* 2019,
170 Bryant *et al.* 2020, Subudhi *et al.* 2023) and found many of ApiAP2 and EELM2 proteins shared
171 across both datasets (**Figure 1B**). Collectively, our results demonstrate a direct association of
172 *Pf*MORC with various chromatin-associated factors, including at least seven ApiAP2 proteins.
173 The potential interactors of *Pf*MORC that we detected in this experiment also included proteins
174 implicated in DNA replication and repair, including the ATP-dependent RNA helicase DBP5
175 (PF3D7_1459000, -*log10 p-value* 0.46) and the DNA helicase 60 DH60 (PF3D7_1227100, -

176 *log10 p-value* 0.41). *Pf*DH60 exhibits DNA and RNA unwinding activities, and its high
177 expression in the trophozoites suggest a role in DNA replication (Pradhan *et al.* 2005). We also
178 identified two putative chromatin-associated proteins, chromodomain-helicase-DNA-binding
179 protein 1 CHD1 (PF3D7_1023900, -*log10 p-value* 0.30) and the SNF2 chromatin-remodeling
180 ATPase ISWI (PF3D7_0624600, -*log10 p-value* 0.001), which are associated with chromosome
181 structure maintenance, DNA replication, DNA repair, and transcription regulation. *Pf*ISWI was
182 previously reported to be associated with *Pf*MORC in the context of *var* gene transcriptional
183 activation during ring stage development (Bryant *et al.* 2020). Gene Ontology (GO) analysis was
184 performed to identify enriched biological processes, cellular components, and molecular
185 functions using a *p-value* cut-off of 0.05. We found significant enrichment of DNA-binding
186 transcription factor activity and mRNA binding, transcription, and regulation of transcription
187 activity (**Supplemental Figure 1E, Supplemental Table 3)**. Overall, we again find that
188 *Pf*MORC forms a link between ApiAP2 TFs and chromatin remodelers (**Figure 1C**).
189

190 **Table 1 –** Potential *Pf*MORC interacting proteins enriched in CoIP eluates and identified in LC–
191 MS/MS from three independent experiments and fold change ≥ 1.5x GFP/3D7.

Protein ID	Annotation	Fold Change	-log *p-value*	Known Function
PF3D7_0519800	EELM2 domain-containing protein	20.79	3.45	-
PF3D7_1139300	AP2 domain transcription factor AP2-G5	20.5	0.22	Repressor of Commitment and Early Gametocyte Development (Shang *et al.* 2021)
PF3D7_1449500	AP2 domain transcription factor AP2-O5	14.99	0.41	Regulator of Mature Ookinete Motility (Modrzynska *et al.* 2017)
PF3D7_1468100	*Pf*MORC	11.76	1.20	
PF3D7_1023900	SNF2 helicase, putative or Chromodomain-helicase-DNA-binding protein 1 homolog, CHD1	10.61	0.30	
PF3D7_1459000	ATP-dependent RNA helicase DBP5	10.24	0.46	
PF3D7_1227100	DNA helicase 60, DH60	6.55	0.41	-
PF3D7_1007700	AP2 domain transcription factor AP2-I	4.65	0.08	Invasion (Santos *et al.* 2017, Josling *et al.* 2020)
PF3D7_1107800	AP2 domain transcription factor	3.11	0.36	Master regulator of parasite growth, chromatin structure and var gene expression (Subudhi *et al.* 2023)
PF3D7_0613800	AP2 domain transcription factor	2.43	0.28	-
PF3D7_0420300	AP2 domain transcription factor (ApiAP2)	2.38	0.48	-
PF3D7_0624600	SNF2 helicase, ISW1	2.09	0.001	*var* gene expression (Bryant *et al.* 2020)
PF3D7_1239200	AP2 domain transcription factor	2.01	0.25	-

192
193
194 ***PfMORC localizes to multigene families in subtelomeric regions***
195 To determine the genome-wide occupancy of the *Pf*MORC chromatin-associated remodeling
196 complex, we used chromatin immunoprecipitation followed by high-throughput sequencing
197 (ChIP-seq). Using purified, crosslinked nuclear extracts, we immunoprecipitated *Pf*MORC

198 from a 3xHA-tagged *Pf*MORC$^{HA\text{-}glmS}$ parasite line (Singh *et al.* 2021) for ChIP-seq at the
199 trophozoite stage (30hpi) and the schizont stage (40hpi) in biological duplicates. These
200 timepoints represent the stages at which *Pf*MORC expression is highest (Singh *et al.* 2021). An
201 independent ChIP-seq experiment in biological duplicate using anti-GFP and a *Pf*MORC^{GFP}
202 parasite line (Singh *et al.* 2021) at the schizont stage was used to confirm our findings,
203 demonstrating that the protein tags do not affect *Pf*MORC immunoprecipitation or genome-
204 wide localization (**Supplemental Figure 2A,B**). As an additional control, we correlated one
205 no-epitope (3D7 wild type), negative control sample using the same anti-HA antibody on
206 unmodified parasite lines for immunoprecipitation (**Supplemental Figure 2A,B;** (Bonnell *et*
207 *al.* 2023)), which resulted in an expected low correlation to the tagged samples. The biological
208 ChIP-seq replicates showed high fold enrichment (Log_2[IP/Input]) (**Supplemental Figure 2C**)
209 and were highly correlated with each other within each timepoint (**Supplemental Figure 2D-**
210 **F**).
211 We identified PfMORC localized to subtelomeric regions on all chromosomes across the *P.*
212 *falciparum* genome, with additional occupancy at internal heterochromatic islands (**Figure**
213 **2A,B**). Within the subtelomeric regions, *Pf*MORC was bound upstream and within the gene
214 bodies of many hypervariable multigene families (**Figure 2C**), including *var* genes
215 (**Supplemental Figure 3**), *rif* genes (**Supplemental Figure 4**), and *stevor* genes
216 (**Supplemental Figure 5**). Predicted binding sites (across both biological replicates) between
217 the 30hpi and 40hpi timepoints showed a high degree of overlap, suggesting that *Pf*MORC
218 binds many of the same regions throughout the later stages of asexual development when
219 *Pf*MORC is highly expressed (**Figure 2D**). The proportion of *Pf*MORC-bound regions was
220 similar across the 5′ upstream region of genes and the gene bodies throughout the genome,
221 including subtelomeric regions (**Figure 2E**). As opposed to the binding of other proteins at the
222 subtelomeric regions, such as the heterochromatin protein 1 (*Pf*HP1) (Flueck *et al.* 2010),
223 *Pf*MORC occupancy is not widespread. Instead, it forms sharp peaks within, and adjacent to,
224 HP1-bound regions (**Figure 2F**), suggesting a unique role for *Pf*MORC in heterochromatin
225 condensation, boundary demarcation, and gene repression.
226 We further defined *Pf*MORC putative gene targets as genes displaying peaks within 2-kb
227 upstream of the ATG start codon or within gene bodies. For those peaks between gene targets
228 in a head-to-head orientation, the closest gene was chosen. This resulted in 149 putative gene
229 targets at 30hpi and 102 gene targets at 40hpi. A close examination of the 84 overlapping genes
230 shows that many are *var* genes, rRNA genes, and genes encoding exported proteins
231 (**Supplemental Table 4**), with GO terms related to cell adhesion, host–pathogen interactions,

232 and antigenic variation (**Supplemental Table 5**). The 65 uniquely bound genes at the 30hpi
233 timepoint showed an enrichment of highly expressed tRNA and rRNAs genes, as well as
234 conserved unknown genes, while those 18 unique to the 40hpi timepoint included a variety of
235 late-stage expressed genes. Transcript abundance (Chappell *et al.* 2020) of the predicted
236 *Pf*MORC gene targets at both the 30hpi and 40hpi timepoints form two major clusters: cluster
237 one being genes expressed at the late ring/early trophozoite stage (10-24hpi) and cluster two at
238 the late schizont stage (40-48hpi) (**Supplemental Figure 6**). This two-cluster gene target
239 pattern of expression mirrors the biphasic pattern of expression by *Pf*MORC, suggesting that
240 *Pf*MORC could have distinct functions, forming complexes with different sets of transcriptional
241 regulators, at various times during asexual proliferation. As determined in other eukaryotic
242 organisms, MORC family proteins do not generally bind DNA in a sequence-specific manner;
243 it is, therefore likely that *Pf*MORC is recruited to these genome-wide regions by sequence-
244 specific transcription factors, such as the ApiAP2 proteins identified in our proteomics results.
245
246 ***Binding sites of PfMORC overlap with ApiAP2 proteins and epigenetic marks***
247 *Pf*MORC has previously been found to interact with several ApiAP2 proteins (Hillier *et al.*
248 2019, Bryant *et al.* 2020, Singh *et al.* 2021), as does the *Toxoplasma* orthologue (Farhat *et al.*
249 2020, Srivastava *et al.* 2023, Antunes *et al.* 2024). We identified a clear overlap between
250 genome-wide *Pf*MORC binding and putatively interacting ApiAP2 proteins using available
251 ChIP-seq datasets. In addition to our protein-protein interaction results (**Table 1**), previous
252 studies have also suggested that *Pf*MORC interacts with a broad array of ApiAP2 TFs, such as
253 *Pf*AP2-G5 , *Pf*AP2-O5, *Pf*AP2-I, PF3D7_1107800, PF3D7_0613800, PF3D7_0420300, and
254 PF3D7_1239200 (Hillier *et al.* 2019, Bryant *et al.* 2020, Subudhi *et al.* 2023). Therefore, we
255 compared binding sites between interacting ApiAP2s and *Pf*MORC using available ChIP-seq
256 data on *Pf*AP2-G5, *Pf*AP2-O5, *Pf*AP2-I, PF3D7_1107800, PF3D7_0613800, PF3D7_1239200
257 (Josling *et al.* 2020, Shang *et al.* 2021, Shang *et al.* 2022). Interestingly, there is a degree of
258 overlap between the binding sites of all six ApiAP2 TFs and *Pf*MORC, suggesting that
259 *Pf*MORC and these ApiAP2 TFs may cooperate in the regulation of gene expression at these
260 loci (**Figure 3A-B; Supplemental Figure 7**). However, the available data cannot differentiate
261 whether all these factors are in one complex together, form multiple smaller heterologous
262 complexes, or are components of separate complexes in individual cells. DNA motif enrichment
263 analysis (Bailey 2021) identified several unique and significant DNA motifs at both the 30hpi
264 and 40hpi timepoints, which suggests that more than one sequence-specific transcription factor
265 may be responsible for recruiting *Pf*MORC to specific genomic regions (**Supplemental Figure**

266 **8**). The common motifs identified across replicates and timepoints are RGTGCAW or
267 TGCACACA, both of which are similar or identical to the *in vitro* and/or *in vivo* DNA-binding
268 motif of *Pf*AP2-I (RGTGCAW) or PF3D7_0420300 (TGCACACA), respectively, suggesting
269 that these ApiAP2 factors may play major roles in *Pf*MORC recruitment (**Supplemental Figure**
270 **8**).
271 In addition to overlapping occupancy with ApiAP2 TFs, we found that *Pf*MORC co-localizes
272 with the depletion of H3K36me2 (**Figure 3C, D**), which is demarcated by the SET2
273 methyltransferase (Jiang *et al.* 2013), both at 30hpi and 40hpi. No other significant co-
274 localization was found between *Pf*MORC and other epigenetic marks (H2A.Z, H3K9ac,
275 H3K4me3, H3K27ac, H3K18ac, H3K9me3, H3K36me2/3, H4K20me3, and H3K4me1)
276 (**Supplemental Figure 9**), suggesting it has a unique binding preference not shared with other
277 heterochromatin markers. Therefore, it is likely that *Pf*MORC co-localizes with other, as yet
278 uncharacterized, epigenetic marks. In summary, *Pf*MORC was found to be recruited to 5`-
279 untranslated regions (UTRs), gene body regions, and subtelomeric regions of repressed,
280 multigene families, and overlaps with other known ApiAP2 binding sites and DNA motifs.
281
282 ***Depletion of PfMORC results in upregulation of late-stage genes associated with invasion***
283 *Pf*MORC association with chromatin remodelers has been shown (Bryant *et al.* 2020), but how
284 *Pf*MORC regulates gene expression in the asexual stage has not been evaluated. In *T. gondii*,
285 the *Tg*MORC:*Tg*ApiAP2 complex acts as a transcriptional repressor of sexual commitment
286 (Farhat *et al.* 2020, Srivastava *et al.* 2023, Antunes *et al.* 2024). Here, we found that *Pf*MORC
287 co-immunoprecipitates with several chromatin remodeling proteins and many ApiAP2
288 transcription factors. Furthermore, our ChIP-seq data revealed that *Pf*MORC is located at
289 subtelomeric regions of the genome. Based on this evidence, we hypothesized that PfMORC
290 may regulate transcriptional changes during blood stage development of the parasite. To knock
291 down the expression of *Pf*MORC (*Pf*MORC-KD), sorbitol-synchronized MORC$^{HA\text{-}glmS}$
292 parasites (22-24hpi) were subjected to 2.5 mM glucosamine (GlcN) treatment for little over 48
293 hours when they reached the trophozoite stage (32hpi ± 3hpi), at which point parasites were
294 harvested for RNA isolation for transcriptomic analysis. In parallel, another flask with
295 *Pf*MORC$^{HA\text{-}glmS}$ parasites was set up without GlcN and used as control for RNA-seq
296 comparison. We previously demonstrated that treatment with 2.5 mM GlcN results in a 50%
297 knockdown of *Pf*MORC protein but does not cause any growth delay; using >2.5 mM GlcN
298 caused a measurable slow growth and reduced parasitemia (Singh *et al.* 2021). Three biological

replicates with and without 2.5 mM GlcN were collected for knockdown transcriptomics to ensure reproducibility.

For each *Pf*MORC RNA-seq sample, gene counts were used to identify the differentially expressed genes (DEGs). Significant threshold parameters were assigned to a p value <0.05, yielding a total of 2558 DEGs (**Supplemental Table 6**). Applying a $\log_2$-fold change cut-off from >1 to <-1 and filtering out pseudogenes reduced this number to 163 DEGs. Among these, 60 genes display more abundant transcripts, whereas 103 genes were reduced relative to control parasites grown without GlcN **(Figure 4A)**. Pathway and functional enrichment analysis yielded several genes from apical organelles. GO analysis revealed gene clusters enriched with molecular function (p-adj = 0.0006) involved in the movement into the host environment and entry into the host, and molecular function of protein binding (p-adj = 0.009) (**Figure 4B, Supplemental Table 7)**. More specifically, upregulated genes implicated in the invasion of merozoites were found to be expressed prematurely upon *Pf*MORC KD; these include several rhoptry-associated genes, notably *Pf*RON2 (PF3D7_1452000) and *Pf*RON3 (PF3D7_1252100). Both *Pf*RON2 and *Pf*RON3 are part of a micronemal complex at the erythrocyte membrane where *Pf*RON2 anchors *Pf*AMA1 to facilitate merozoite invasion (Srinivasan *et al.* 2013). In addition, *Pf*SUB3 (PF3D7_0507200), *Pf*SERA5 (PF3D7_0207600) and *Pf*DPAP3 (PF3D7_0404700), all of which are critical for schizont rupture (Yeoh *et al.* 2007, Arastu-Kapur *et al.* 2008), were among the upregulated DEGs (**Figure 4C**). In general, we found that depletion of *Pf*MORC leads to upregulation of invasion-related genes, which suggests that *Pf*MORC has an additional function in the regulation of genes specifically associated with red blood cell invasion.

PfMORC-depleted parasites downregulate hypervariable gene families

Among the genes with reduced mRNA abundance, DEGs linked to cytoadherence, antigenic variation and interaction with host (**Figure 4B and D**) where over-represented in the GO analysis. Many of the genes enriched in the downregulated group belong to the clonally variant *var* multigene family that represents 60 members encoding the *P. falciparum* erythrocyte membrane proteins (*Pf*EMP1), which upon switching expression, aid in pathogenesis and immune evasion (Guizetti and Scherf 2013). Furthermore, a cluster of genes encoding putative exported proteins were also enriched including members of the exported protein family (EPFs), *Plasmodium* exported protein (hyp), and *Plasmodium* exported protein (PHISTa/b). Other significantly overrepresented downregulated genes belonged to serine/threonine protein kinases, the FIKK family (Ward *et al.* 2004), most of which are exported to the RBC, and

333 Maurer's clefts two transmembrane proteins (Pfmc-2TM) (**Figure 4D**). Notably, expressed
334 proteins are conserved across the *Plasmodium* family and remain confined to the hypervariable
335 subtelomeric region of *P. falciparum* chromosomes (Sargeant *et al.* 2006).
336
337 ***Comparison of ChIP-seq gene targets and DEGs by RNA-seq***
338 To identify whether genes found to be dysregulated after PfMORC knockdown are associated
339 with the genome-wide occupancy of *Pf*MORC, we correlated the gene targets identified by
340 ChIP-seq with the DEGs determined by RNA-seq. We identified a total of 135 gene targets
341 from the 30hpi ChIP-seq timepoint, 72 gene targets from the 40hpi ChIP-seq timepoint, and
342 163 DEGs by RNA-seq. The low correlation between the ChIP-seq gene targets and the RNA-
343 seq DEGs suggest that *Pf*MORC genome-wide occupancy is more likely involved in chromatin
344 structure, rather than specific regulation of gene targets (**Figure 4E**). Likely, *Pf*MORC localizes
345 to these sites to aid in chromatin condensation, as shown in other eukaryotic systems (Zhang *et*
346 *al.* 2019, Zhong *et al.* 2023).
347

348 ## Discussion

349 Periodic gene expression during the asexual blood stage directly corresponds to the timing in
350 which gene products are needed (Bozdech *et al.* 2003) and shows oscillation patterns associated
351 with circadian rhythms (Smith *et al.* 2020, Subudhi *et al.* 2020). Transcription factors are
352 critical regulators of this dynamic pattern in concert with epigenetic regulators and genome-
353 wide changes to chromatin structure (Painter *et al.* 2011, Toenhake *et al.* 2018, Jeninga *et al.*
354 2019, Hollin *et al.* 2021). The ApiAP2 family members display unique binding preferences in
355 the genome (Campbell *et al.* 2010), undergo stage-specific expression (Painter *et al.* 2011), and
356 have been identified to regulate virtually all stages of development across multiple *Plasmodium*
357 species (Jeninga *et al.* 2019). To date, ApiAP2 proteins have been reported in transcriptional
358 silencing of clonally variant genes, regulation of invasion genes, and sexual commitment, acting
359 through interaction with other epigenetic factors, such as heterochromatin protein 1 [*Pf*HP1
360 (Flueck *et al.* 2010, Brancucci *et al.* 2014, Fraschka *et al.* 2018)], bromodomain protein 1
361 [*Pf*BDP1 (Santos *et al.* 2017, Josling *et al.* 2020, Quinn *et al.* 2022)], or general control non-
362 depressible 5 [*Pf*GCN5 (Miao *et al.* 2021)]. Despite the known DNA-binding sites of many
363 ApiAP2 proteins (Flueck *et al.* 2010, Santos *et al.* 2017, Sierra-Miranda *et al.* 2017, Josling *et*
364 *al.* 2020, Carrington *et al.* 2021, Shang *et al.* 2021, Singh *et al.* 2021, Russell *et al.* 2022, Shang
365 *et al.* 2022, Bonnell *et al.* 2023), limited information is available for other accessory proteins.

366 Recently, the *T. gondii* orthologue *Tg*MORC was identified in a complex with HDAC1,
367 AP2XII-2, and AP2XII-1:AP2XI-2and orchestrates epigenetic rewiring of sexual gene
368 transcription (Farhat *et al.* 2020, Srivastava *et al.* 2023, Antunes *et al.* 2024). In *P. falciparum*,
369 *Pf*MORC has been copurified with several ApiAP2 proteins, as shown by different independent
370 studies (Hillier *et al.* 2019, Bryant *et al.* 2020, Singh *et al.* 2021).
371 In this study, we used an integrated multi-omics approach to explore the function of *Pf*MORC
372 during asexual blood stage development. Using immunoaffinity-based purification, we
373 identified a number of nuclear proteins that interact with *Pf*MORC. More specifically, *Pf*MORC
374 was associated with *Pf*AP2-G5, which is essential for gametocytogenesis (Shang *et al.* 2021),
375 *Pf*AP2-I, which is required for the expression of many invasion-related genes (Santos *et al.*
376 2017), and with other ApiAP2 TFs of unknown function (*Pf*AP2-O5, PF3D7_1107800,
377 PF3D7_0613800, PF3D7_0420300, and PF3D7_1239200). The identification of *Pf*ISW1 and
378 *Pf*CHD1 in association with *Pf*MORC strengthens the link between *Pf*MORC and chromatin
379 remodeling. This finding suggests that *Pf*MORC may participate in regulating chromatin
380 structure and gene expression during the IDC, notably the specific regulation of *var* genes. We
381 note that some nuclear proteins were not identified in this study despite their documented
382 interaction with *Pf*MORC in other studies (Hillier *et al.* 2019, Bryant *et al.* 2020, Singh *et al.*
383 2021, Subudhi *et al.* 2023). This may be due to differences in experimental conditions between
384 the various studies, and to the low abundance of the proteins. Despite this, our identification of
385 several nuclear proteins in complex with *Pf*MORC provides insights into potential interactions
386 and regulatory mechanisms underlying gene regulation and chromatin remodeling in *P.*
387 *falciparum*; this may have implications for developing new strategies to combat malaria.
388 In other eukaryotes, MORC proteins function in gene repression and chromatin compaction at
389 heterochromatic regions (Koch *et al.* 2017). Therefore, to determine if *Pf*MORC localizes to
390 heterochromatic regions across the *P. falciparum* genome, we performed ChIP-seq assays with
391 $MORC^{HA\text{-}glmS}$ parasites during peak PfMORC expression (trophozoite and schizont stages). In
392 general, *Pf*MORC occupied regions 5`–upstream of the ATG start site or was bound within
393 coding region, irrespective of the developmental stage. Most importantly, *Pf*MORC peaks were
394 reproducibly detected in subtelomeric regions containing hypervariable multigene families,
395 including the *var* genes, consistent with the findings that *Pf*MORC localized to *var* gene
396 promoters as reported using dCas9 (Bryant *et al.* 2020). The specific binding pattern of *Pf*MORC
397 near or within *Pf*HP1-bound regions suggests two related critical functions: heterochromatin
398 condensation and gene repression. It is possible that *Pf*MORC changes the nucleosome
399 landscape either by direct association or by binding to different chromatin remodelers. Recent

work in *Arabidopsis* has further confirmed the importance of *At*MORC paralogs in gene regulation by chromatin compaction (Zhong *et al.* 2023), which resembles the function of *Pf*MORC in *P. falciparum*. Interestingly, in *T. gondii*, the major function of *Tg*MORC was in the repression of sex-determination genes (Farhat *et al.* 2020), suggesting MORC family proteins have the capacity to perform diverse functions across eukaryotic organisms. Future studies should determine if *Pf*MORC depletion similarly influences the rate of sexual commitment to *P. falciparum* gametocytogenesis, which is known to be regulated by epigenetic mechanisms. Role of *Pf*HP1 has been shown in regulating sexual commitment by repressing *Pf*AP2-G and virulence genes expression (Brancucci *et al.* 2014), whereas gametocyte development 1 (*Pf*GDV1) displaces *Pf*HP1 itself and induces asexual developing parasites to sexual differentiation (Filarsky *et al.* 2018).

We also compared *Pf*MORC occupancy with available ChIP-seq data for the interacting ApiAP2 proteins. Interestingly, our analysis revealed a significant overlap between the binding sites of all ChIP-ed ApiAP2 proteins with *Pf*MORC, suggesting a cooperative role in gene regulation. We also identified enriched motifs similar to those bound by our ApiAP2 proteins of interest, further suggesting the functional cooperation between *Pf*MORC and ApiAP2 proteins. Of note, only one of the seven ApiAP2 of interest in our study has not been ChIP-ed to date (PF3D7_0420300) (Shang *et al.* 2022). However, we found an enrichment of the DNA motif (TGCACACA) at *Pf*MORC-bound sites. This motif is bound *in vitro* by PF3D7_0420300 (Bonnell *et al.* 2023), suggesting that this ApiAP2 protein may localize to these regions. Overall, since these seven ApiAP2 proteins are expressed at distinct time points during the *P. falciparum* cycle (Bozdech *et al.* 2003) and regulate different sets of genes (Santos *et al.* 2017, Josling *et al.* 2020, Shang *et al.* 2021, Shang *et al.* 2022, Subudhi *et al.* 2023), we believe this indicates a variety of functions for *Pf*MORC at different stages. In addition, a recent study in *Arabidopsis* reported that *At*MORC-mediated regulation of transcription may be due to both direct chromatin interactions and indirect association via sequence-specific transcription factors (Zhong *et al.* 2023) consistent with a complex landscape of chromatin remodeling by MORC proteins. We also interrogated the co-localization of *Pf*MORC and numerous epigenetic profiles (H2A.Z, H3K9ac, H3K4me3, H3K27ac, H3K18ac, H3K9me3, H3K36me2/3, H4K20me3, and H3K4me1), with a specific focus on H3K36me2, since this histone modification has been shown to act as a global repressive effector in *P. falciparum* (Karmodiya *et al.* 2015) and other organisms (Strahl *et al.* 2002, Wagner and Carpenter 2012). Interestingly, we did not find a strong co-localization with any of these epigenetic marks, suggesting a unique role of the

433 epigenetic landscape on *Pf*MORC global occupancy. Therefore, the functional association
434 between *Pf*MORC and a specific, unknown epigenetic mark remains to be determined.
435 Before this work, there was no direct evidence correlating *Pf*MORC-mediated transcriptional
436 changes during the IDC of *P. falciparum*. Therefore, we investigated the differentially
437 expressed genes (DEGs) in *Pf*MORC knockdown parasites and found two distinct subsets of
438 enriched genes. The upregulated DEGs were enriched with genes related to invasion, while the
439 downregulated DEGs belong to hypervariable genes associated with parasite virulence. It
440 suggests that *Pf*MORC has very dynamic function across *Plasmodium* asexual cycle as we also
441 identified *Pf*AP2-I in CoIPed proteins, which is shown to regulate invasive gene transcription
442 (Santos *et al.* 2017). Overall, our data with *Pf*MORC-KD revealed a change in the expression
443 of both antigenically variable and invasion-related genes. Expression of clonally variant genes
444 occurs in a different but tightly regulated manner in IDC (Scherf *et al.* 1998, Scherf *et al.* 2008),
445 which, in the light of our data, may be regulated by *Pf*MORC occupancy. Data regarding
446 changes in *var* gene expression are difficult to interpret, as the KD experiments were performed
447 on a parasite that had not been recloned and may therefore express more than one *var* gene.
448 Single-cell experiments would be needed to clarify the effect of *Pf*MORC KD on *var* gene
449 regulation. We were surprised by the small number of DEGs detected upon knockdown of
450 *Pf*MORC, which we believe may be due to incomplete knockdown.
451 We previously showed that parasites in which *Pf*MORC is knocked-down display reduced
452 sensitivity to melatonin (Singh et al. 2021). This prompted us to investigate if overall gene
453 expression in *Pf*MORC KD parasites is affected by melatonin treatment. We detected only very
454 slight changes **(Supplemental Figure 10A-D)**, suggesting that melatonin does not exert its
455 effect on gene expression through *Pf*MORC, or at least that the latter protein plays a minor role
456 in the process.
457 Overall, this study shows that *Pf*MORC interacts with different ApiAP2 TFs, in line with
458 previous studies (Hillier *et al.* 2019, Bryant *et al.* 2020, Singh *et al.* 2021, Subudhi *et al.* 2023)
459 and a recently published parallel study (Chahine *et al.* 2023). Furthermore, we found that
460 *Pf*MORC is localized at sub-telomeric regions and contains significant overlap with the
461 bindingsites of several ApiAP2 transcription factors. Our results support a role for *Pf*MORC in
462 the regulation of hypervariable genes that are essential for *Plasmodium* virulence and rhoptry
463 genes critical to red blood cell invasion. Collectively, our data identify an important role for
464 *Pf*MORC in chromatin organization, as well as in the epigenetic regulation of gene expression
465 through regulatory complexes with an array of transcription factors, making it an attractive drug
466 target.

467 # Materials and Methods

468 ***Plasmodium falciparum* culture**

469 The *P. falciparum* strains were cultured at 37°C in RPMI 1640 medium supplemented with
470 0.5% Albumax II (Gibco) (Trager and Jensen 1976). Parasites were grown under a 5% CO_2,
471 5% O_2, and 90% N_2 atmosphere. Cultures were synchronized with 5% sorbitol (Lambros and
472 Vanderberg 1979).

473

474 **Coimmunoprecipitation and mass spectrometry**

475 Infected erythrocytes at the trophozoite stage were collected from culture and washed twice in
476 1x phosphate-buffered saline (PBS). The culture pellet was suspended in PBS containing 0.05%
477 (w/v) saponin to lyse the erythrocyte membrane and centrifuged at 8,000 × g for 10 min. The
478 supernatant was discarded, and the parasite pellet was washed 3 times in cold PBS. To perform
479 the co-immunoprecipitation, we followed the manufacturer protocol (ChromoTek, gta-20).
480 Samples were lysed in modified RIPA buffer (50 mM Tris, pH 7.5, 150 mM NaCl, 0.5% sodium
481 deoxycholate, 1% Nonidet P-40, 10 µg/ml aprotinin, 10 µg/ml leupeptin, 10 µg/ml, 1 mM
482 phenylmethylsulfonyl fluoride, benzamidine) for 30 min on ice. The lysate was precleared with
483 50 µl of protein A/G-Agarose beads at 4°C for 1 h and clarified by centrifugation at 10,000 × g
484 for 10 min. The precleared lysate was incubated overnigh with an anti-GFP-Trap-A beads
485 (ChromoTek, gta-20) antibody. The magnetic beads were then pelleted using a magnet
486 (Invitrogen), and the beads were washed extensively using wash buffer (50 mM Tris, pH 7.5,
487 150 mM NaCl, 0.5% sodium deoxycholate, 1% Nonidet P-40) to minimize the detection of non-
488 specific proteins. To elute the immunoprecipitated proteins, the magnetic beads were
489 resuspended in 2X SDS loading buffer and resolved by SDS–PAGE. Following SDS–PAGE,
490 the whole gel band for each sample was excised and further analysed by mass spectrometry.
491 We used a service provider (CEFAP core-facility de Espectometria de Massa) to analyse GFP-
492 coimmunoprecipitated proteins.

493

494 **In-gel digestion and peptide desalting**

495 Protein bands from polyacrylamide gels were cut into pieces (approximately 1 mm^3),
496 transferred to a clean 1.5 ml low binding tube and washed with washing solution (40%
497 acetonitrile, 50 mM ammonium bicarbonate) until the bands were completely distained, and
498 dehydrated with ACN 100% for 5 min followed by vacuum centrifugation. Proteins were then
499 reduced with 10 mM dithiothreitol (DTT) in 50 mM ammonium bicarbonate and incubated for

500 45 minutes at 56°C. Protein alkylation was performed with 55 mM iodoacetamide (IAA) in 50
501 mM ammonium bicarbonate and incubated for 30 minutes at room temperature. Proteins were
502 digested into peptides by trypsin overnight reaction at 37°C. The trypsin reaction was stopped
503 with 10% TFA (1% TFA final concentration). The supernatant was collected into a new tube.
504 Extraction buffer (40% ACN/0.1% TFA) was added to the gel pieces and incubated for 15
505 minutes on a thermomixer at room temperature. The supernatant was transferred to the same
506 microtube. The peptide extraction was performed twice and then dried in a vacuum centrifuge.
507 Peptides were resuspended in 0.1% TFA for desalting.
508

509 **Nano LC–MS/MS analysis**

510 The LC–MS/MS system employed was an Easy-nano LC 1200 system (Thermo Fisher
511 Scientific Corp) coupled to an Orbitrap Fusion Lumos mass spectrometer equipped with a
512 nanospray source (Thermo Fisher Scientific Corp). Samples were loaded onto a trapping
513 column (Acclaim PepMap 0.075 mm, 2 cm, C18, 3 µm, 100 A; Thermo Fisher Scientific Corp.)
514 in line with a nano-LC column (Acclaim PepMap RSLC 0.050 mm, 15 cm, C18, 2 µm, 100 A;
515 Thermo Fisher Scientific Corp.). The gradient was 5-28% solvent B (A 0.1% FA; B 90% ACN,
516 0.1% FA) for 25 minutes, 28-40% B for 3 minutes, 40-95% B for 2 minutes and 95% B for 12
517 minutes at 300 nL/min. Orbitrap Fusion Lumos mass spectrometer operated in positive mode.
518 The full MS scan had an automatic gain control (AGC) of 5 x 105 ions and a maximum filling
519 time of 50 ms. Each MS scan was acquired at 120K full width half maximum (FWHM) high
520 resolution in the Orbitrap with a mass range of m/z 400-1600 Da. High-resolution dissociation
521 (HCD) with a normalized collision energy set at 30 was used for fragmentation. The resulting
522 MS/MS fragment ions were detected in the Orbitrap mass analyser at a resolution of 30,000.
523 An AGC of 5 x 104 ions and a maximum injection time of 54 ms were used. All raw data were
524 accessed in Xcalibur software (Thermo Scientific).
525

526 **Database searches and bioinformatics analyses**

527 Raw files were imported into MaxQuant version 1.6.17.0 for protein identification and
528 quantification. For protein identification in MaxQuant, the database search engine Andromeda
529 was used against the UniProt *P. falciparum* 3D7 strain (March 2021, 5388 entries release). The
530 following parameters were used: carbamidomethylation of cysteine (57.021464 Da) as a fixed
531 modification, oxidation of methionine (15.994915 Da) and N-terminal acetylation protein
532 (42.010565 Da) were selected as variable modifications. Enzyme specificity was set to full
533 trypsin with a maximum of two missed cleavages. The minimum peptide length was set to 7

534 amino acids. For label-free quantification, the “match between runs” feature in MaxQuant was
535 used, which is able to identify the transfer between samples based on the retention time and
536 accurate mass, with a 0.7-minute match time window and 20-minute alignment time window.
537 Label-free quantification was performed using MaxQuant software with the “match between
538 run” and iBAQ features activated. Protein LFQ and iBAQ ratios were calculated for the two
539 conditions, and the protein IDs were divided accordingly. The mass spectrometry proteomics
540 data have been deposited to the ProteomeXchange Consortium via the PRIDE (Perez-Riverol
541 *et al.* 2022) partner repository with the dataset identifier PXD036092. PlasmoDB database was
542 used to perform GO analysis.
543
544 **Total RNA extraction and RNAseq**
545 Infected RBCs containing tightly synchronized trophozoite stage parasites (32 hpi ± 3 h) were
546 harvested and resuspended in TRIzol (Thermo Fisher Scientific). Total RNA was extracted
547 following the manufacturer’s protocol, and an RNA cleanup kit (Qiagen) was used to achieve
548 high-purity RNA. The isolated RNA was quantified using a NanoDrop ND-1000 UV/Vis
549 spectrophotometer, and RNA quality was determined using an RNA ScreenTape System
550 (Agilent 2200 TapeStation). Total RNA (10000 ng) from each sample was stabilized in
551 RNAStable (Biomatrica) and sent to the Micromon Genomics facility at Monash University for
552 next-generation sequencing.
553 RNA samples were prepared using the MGITech RNA Directional Library Prep Kit V2 (Item
554 No. 1000006385), as per the manufacturer's instructions, with the following parameters: input
555 RNA: 50 ng, fragmentation: target of 200 bp-400 bp, 87 °C for 6 mins, adapter clean-up: 200
556 bp-400 bp and library amplification cycles: 16. Libraries were assessed for quantity using the
557 Invitrogen Qubit and dsDNA HS chemistry (Item No. Q33230) and quality/quality using the
558 Agilent Fragment Analyser 5200 with the HS NGS Fragment Kit (Item No. DNF-473-0500).
559 The libraries were pooled in equimolar concentrations and sequenced using an MGITech
560 DNBSEQ-G400RS sequencing instrument with High-Throughput Sequencing Set (FCL
561 PE100, Item No. 1000016950) chemistry.
562 The quality of the RNA-seq libraries was evaluated using the FastQC tool. Next, we used
563 Salmon (V1.9.0) (Patro *et al.* 2017) quant with default arguments to quantify the expression of
564 all transcripts in the PlasmoDB release-58 Pfalciparum3D7 genome. The transcript expression
565 was summarized to gene-level expression with tximport 1.22.0 (Soneson *et al.* 2015). Finally,
566 the gene counts were used to detect differentially expressed genes (DEGs) with DESeq2

567 (1.34.0) (Love *et al.* 2014). Furthermore, only genes with an >1 $\log_2$ fold change and adjusted
568 *p-value* <0.1 were considered significant for further analysis.
569
570 **Chromatin immunoprecipitation followed by high-throughput sequencing (ChIP-seq)**
571 PfMORC ChIP-seq was performed similarly to previously published ChIP-seq experiments in
572 *Plasmodium falciparum* (Josling *et al.* 2020, Singh *et al.* 2021, Russell *et al.* 2022). Five
573 samples in total were collected: biological duplicates using the PfMORC$^{HA\text{-}glmS}$ parasite line at
574 the trophozoite stage [30 hpi], biological duplicates using the PfMORC^{HA} parasite line at the
575 schizont stage [40 hpi], and a single replicate using the PfMORC^{GFP} parasite line at the schizont
576 stage [40 hpi]. In brief, the protocol includes five steps: (1) Treated with 1% formaldehyde to
577 crosslink the suspended PfMORC$^{HA\text{-}glmS}$ (or PfMORC^{GFP}) parasite cultures (at least 10^8
578 trophozoite- or schizont-stage parasites synchronized with 10% sorbitol more than one cycle
579 prior) at 37°C for 10 minutes; (2) Collected parasite nuclei using prechilled glass Dounce
580 homogenizer for 100 strokes per 10^9 trophozoites/schizonts; (3) Lysed parasite nuclei and
581 mechanically sheared chromatin until sufficiently sheared using Covaris Focus-Ultrasonicator
582 M220 (5% duty cycle, 75 W peak incident power, 200 cycles per burst, 7°C, for 5 minutes). (4)
583 We collected 10% of each sample for the non-immunoprecipitated "input" control and then
584 immunoprecipitated the remaining 90% of each sample. The remaining 90% of each sample
585 was immunoprecipitated with 1:1000 anti-HA antibody (0.5 mg/mL Roche Rat Anti-HA High
586 Affinity [11867423001]) or 1:1000 anti-GFP antibody (0.1 mg/mL Abcam Rabbit Anti-GFP
587 [Ab290]) overnight at 4°C with rotation. (5) DNA was purified after reverse crosslinking using
588 a MinElute column (Qiagen) as directed and quantified by a Qubit fluorometer (Invitrogen).
589
590 **ChIP-seq library prep for Illumina sequencing**
591 The PfMORC ChIP-seq libraries were performed similarly to previously published ChIP-seq
592 experiments in *Plasmodium falciparum* (Josling *et al.* 2020, Singh *et al.* 2021, Russell *et al.*
593 2022). DNA sequencing libraries were prepared for high-throughput Illumina sequencing on
594 the NextSeq 2000 with the 150 x 150 single-end mode. The library prep underwent 12 rounds
595 of amplification using KAPA HiFi polymerase. Completed libraries were quantified using the
596 Qubit fluorometer (Invitrogen) for high-sensitivity DNA and library sequence length by the
597 Agilent TapeStation 4150.
598
599 **ChIP-seq data analysis and peak calling**

600 The MORC ChIP-seq datasets were analysed similar to previously published ChIP-seq
601 experiments in *Plasmodium falciparum* **(Josling *et al.* 2020, Singh *et al.* 2021, Russell *et al.*
602 **2022)**. Raw sequencing reads were trimmed (Trimmomatic v0.32.3) to remove Illumina adaptor
603 sequences and low-quality reads below 30 Phred (SLIDINGWINDOW: 4:30). FastQC
604 (v0.11.9) was used to check the quality after trimming. Processed reads were then mapped to
605 the *P. falciparum* genome (release 57) using BWA-MEM (v0.7.17.2) simple Illumina mode
606 with multiple mapped reads filtered out (MAPQ=1). Once the sequences were mapped, MACS2
607 (v2.2.7.1) was used to call peaks with each biological replicate and its paired input sample using
608 a standard significance cut-off (q-value=0.01). Using BedTools Multiple Intersect (v2.29.2),
609 the narrow peak output file for each replicate was overlapped to identify the significant peaks
610 in the overlap between both ChIP-seq biological replicates. The overlapping regions were then
611 used to identify an enriched DNA motif (STREME Meme Suite: (Bailey 2021), and putative
612 gene targets of PfMORC were defined as genes with peaks within 2 kb upstream of the gene
613 target ATG start codon or peaks within gene bodies. In a situation with any peaks between gene
614 targets in a head-to-head orientation, the closest gene was chosen.

615 **Data availability**

616 The mass spectrometry proteomics data have been deposited to the ProteomeXchange
617 Consortium via the PRIDE partner repository with the dataset identifier PXD044256. All ChIP-
618 seq samples were submitted to GEO, and a GEO submission ID (GSE239393) was obtained for
619 this section. Additionally, submit all the relevant ChIP-seq files to Zenodo, since UCSC
620 browser doesn't easily work from *Plasmodium falciparum* data. All RNA-seq samples were
621 submitted to GEO, and a GEO submission ID (GSE241313) was obtained for this section.

622

623 **Author Contributions**

624 MKS, CRSG, and ML designed the experiments. MKS, VAB, VFS and MSM performed the
625 experiments, and data were analyzed by MKS, VAB, ITS, GP, ML and CRSG. The primary
626 manuscript was written by MKS and VAB and proofread by CD, ML and CRSG.

627

628 **Acknowledgments**

629 This work was supported by grants from Fundação de Amparo a Pesquisa de São Paulo
630 (FAPESP) to C.R.S.G. (2017/08684-7 and 2018/07177-7) and to M.K.S (2019/09490-7).
631 C.R.S.G. is supported by "bolsa de produtividade" by CNPq. This work was supported by the
632 National Institutes of Health grant number R01-AI125565 to M.L. and T32-GM125592 to
633 V.A.B. We are grateful to Haemocentro Hospital do Servidor Público for providing blood and
634 plasma. Work in C.D. laboratory is supported by RMIT University and by grant APP2003712
635 from the Australian Health and Medical Research Council (NHMRC). We thank Prof. Paolo
636 Di Mascio and Graziella E. Ronsein for the Mass spectrometry analyses performed at the Redox
637 Proteomics Core of the Mass Spectrometry Resource at Chemistry Institute, University of São
638 Paulo (FAPESP 2012/12663-1, 2016/00696-3, 2023/00995-4, CEPID Redoxoma 2013/07937-
639 8), and Dr. Mariana P. Massafera for her technical assistance.

640

641 **Additional Information**

642 Additional figures and tables are provided separately in Supplemental Figures and
643 Supplemental Tables.

644

645 **Competing Financial Interests**

646 The authors declare no competing financial interests.

References

Antunes, A. V., M. Shahinas, C. Swale, D. C. Farhat, C. Ramakrishnan, C. Bruley, D. Cannella, M. G. Robert, C. Corrao, Y. Coute, A. B. Hehl, A. Bougdour, I. Coppens and M. A. Hakimi (2024). "In vitro production of cat-restricted Toxoplasma pre-sexual stages." Nature **625**(7994): 366-376.

Arastu-Kapur, S., E. L. Ponder, U. P. Fonovic, S. Yeoh, F. Yuan, M. Fonovic, M. Grainger, C. I. Phillips, J. C. Powers and M. Bogyo (2008). "Identification of proteases that regulate erythrocyte rupture by the malaria parasite Plasmodium falciparum." Nat Chem Biol **4**(3): 203-213.

Bailey, T. L. (2021). "STREME: Accurate and versatile sequence motif discovery." Bioinformatics **37**(18): 2834-2840.

Balaji, S., M. M. Babu, L. M. Iyer and L. Aravind (2005). "Discovery of the principal specific transcription factors of Apicomplexa and their implication for the evolution of the AP2-integrase DNA binding domains." Nucleic Acids Res **33**(13): 3994-4006.

Bonnell, V. A., Y. Zhang, J. Alan S. Brown, J. Horton, G. A. Josling, T.-P. Chiu, R. Rohs, S. Mahony, R. Gordân and M. Llinás (2023). "DNA sequence context and the chromatin landscape differentiate sequence-specific transcription factor binding in the human malaria parasite, Plasmodium falciparum." bioRxiv: 2023.2003.2031.535174.

Bordiya, Y., Y. Zheng, J. C. Nam, A. C. Bonnard, H. W. Choi, B. K. Lee, J. Kim, D. F. Klessig, Z. Fei and H. G. Kang (2016). "Pathogen Infection and MORC Proteins Affect Chromatin Accessibility of Transposable Elements and Expression of Their Proximal Genes in Arabidopsis." Mol Plant Microbe Interact **29**(9): 674-687.

Bozdech, Z., M. Llinas, B. L. Pulliam, E. D. Wong, J. Zhu and J. L. DeRisi (2003). "The transcriptome of the intraerythrocytic developmental cycle of Plasmodium falciparum." PLoS Biol **1**(1): E5.

Brancucci, N. M. B., N. L. Bertschi, L. Zhu, I. Niederwieser, W. H. Chin, R. Wampfler, C. Freymond, M. Rottmann, I. Felger, Z. Bozdech and T. S. Voss (2014). "Heterochromatin protein 1 secures survival and transmission of malaria parasites." Cell Host Microbe **16**(2): 165-176.

Bryant, J. M., S. Baumgarten, F. Dingli, D. Loew, A. Sinha, A. Claes, P. R. Preiser, P. C. Dedon and A. Scherf (2020). "Exploring the virulence gene interactome with CRISPR/dCas9 in the human malaria parasite." Mol Syst Biol **16**(8): e9569.

Bushell, E., A. R. Gomes, T. Sanderson, B. Anar, G. Girling, C. Herd, T. Metcalf, K. Modrzynska, F. Schwach, R. E. Martin, M. W. Mather, G. I. McFadden, L. Parts, G. G. Rutledge, A. B. Vaidya, K. Wengelnik, J. C. Rayner and O. Billker (2017). "Functional Profiling of a Plasmodium Genome Reveals an Abundance of Essential Genes." Cell **170**(2): 260-272 e268.

Campbell, T. L., E. K. De Silva, K. L. Olszewski, O. Elemento and M. Llinas (2010). "Identification and genome-wide prediction of DNA binding specificities for the ApiAP2 family of regulators from the malaria parasite." PLoS Pathog **6**(10): e1001165.

Carrington, E., R. H. M. Cooijmans, D. Keller, C. G. Toenhake, R. Bartfai and T. S. Voss (2021). "The ApiAP2 factor PfAP2-HC is an integral component of heterochromatin in the malaria parasite Plasmodium falciparum." iScience **24**(5): 102444.

Chahine, Z., M. Gupta, T. Lenz, T. Hollin, S. Abel, C. A. S. Banks, A. Saraf, J. Prudhomme, L. Florens and K. G. Le Roch (2023). PfMORC protein regulates chromatin accessibility and transcriptional repression in the human malaria parasite, *P. falciparum*, Cold Spring Harbor Laboratory.

Chappell, L., P. Ross, L. Orchard, T. J. Russell, T. D. Otto, M. Berriman, J. C. Rayner and M. Llinas (2020). "Refining the transcriptome of the human malaria parasite Plasmodium falciparum using amplification-free RNA-seq." BMC Genomics **21**(1): 395.

Cowman, A. F., D. Berry and J. Baum (2012). "The cellular and molecular basis for malaria parasite invasion of the human red blood cell." J Cell Biol **198**(6): 961-971.

Dong, W., A. Vannozzi, F. Chen, Y. Hu, Z. Chen and L. Zhang (2018). "MORC Domain Definition and Evolutionary Analysis of the MORC Gene Family in Green Plants." Genome Biol Evol **10**(7): 1730-1744.

Farhat, D. C., C. Swale, C. Dard, D. Cannella, P. Ortet, M. Barakat, F. Sindikubwabo, L. Belmudes, P. J. De Bock, Y. Coute, A. Bougdour and M. A. Hakimi (2020). "A MORC-driven transcriptional switch

controls Toxoplasma developmental trajectories and sexual commitment." Nat Microbiol **5**(4): 570-583.
Filarsky, M., S. A. Fraschka, I. Niederwieser, N. M. B. Brancucci, E. Carrington, E. Carrio, S. Moes, P. Jenoe, R. Bartfai and T. S. Voss (2018). "GDV1 induces sexual commitment of malaria parasites by antagonizing HP1-dependent gene silencing." Science **359**(6381): 1259-1263.
Flueck, C., R. Bartfai, I. Niederwieser, K. Witmer, B. T. Alako, S. Moes, Z. Bozdech, P. Jenoe, H. G. Stunnenberg and T. S. Voss (2010). "A major role for the Plasmodium falciparum ApiAP2 protein PfSIP2 in chromosome end biology." PLoS Pathog **6**(2): e1000784.
Fraschka, S. A., M. Filarsky, R. Hoo, I. Niederwieser, X. Y. Yam, N. M. B. Brancucci, F. Mohring, A. T. Mushunje, X. Huang, P. R. Christensen, F. Nosten, Z. Bozdech, B. Russell, R. W. Moon, M. Marti, P. R. Preiser, R. Bartfai and T. S. Voss (2018). "Comparative Heterochromatin Profiling Reveals Conserved and Unique Epigenome Signatures Linked to Adaptation and Development of Malaria Parasites." Cell Host Microbe **23**(3): 407-420 e408.
Gardner, M. J., N. Hall, E. Fung, O. White, M. Berriman, R. W. Hyman, J. M. Carlton, A. Pain, K. E. Nelson, S. Bowman, I. T. Paulsen, K. James, J. A. Eisen, K. Rutherford, S. L. Salzberg, A. Craig, S. Kyes, M. S. Chan, V. Nene, S. J. Shallom, B. Suh, J. Peterson, S. Angiuoli, M. Pertea, J. Allen, J. Selengut, D. Haft, M. W. Mather, A. B. Vaidya, D. M. Martin, A. H. Fairlamb, M. J. Fraunholz, D. S. Roos, S. A. Ralph, G. I. McFadden, L. M. Cummings, G. M. Subramanian, C. Mungall, J. C. Venter, D. J. Carucci, S. L. Hoffman, C. Newbold, R. W. Davis, C. M. Fraser and B. Barrell (2002). "Genome sequence of the human malaria parasite Plasmodium falciparum." Nature **419**(6906): 498-511.
Guizetti, J. and A. Scherf (2013). "Silence, activate, poise and switch! Mechanisms of antigenic variation in Plasmodium falciparum." Cell Microbiol **15**(5): 718-726.
Harris, M. T., V. Jeffers, J. Martynowicz, J. D. True, A. L. Mosley and W. J. Sullivan, Jr. (2019). "A novel GCN5b lysine acetyltransferase complex associates with distinct transcription factors in the protozoan parasite Toxoplasma gondii." Mol Biochem Parasitol **232**: 111203.
Hillier, C., M. Pardo, L. Yu, E. Bushell, T. Sanderson, T. Metcalf, C. Herd, B. Anar, J. C. Rayner, O. Billker and J. S. Choudhary (2019). "Landscape of the Plasmodium Interactome Reveals Both Conserved and Species-Specific Functionality." Cell Rep **28**(6): 1635-1647 e1635.
Hoeijmakers, W. A. M., J. Miao, S. Schmidt, C. G. Toenhake, S. Shrestha, J. Venhuizen, R. Henderson, J. Birnbaum, S. Ghidelli-Disse, G. Drewes, L. Cui, H. G. Stunnenberg, T. Spielmann and R. Bartfai (2019). "Epigenetic reader complexes of the human malaria parasite, Plasmodium falciparum." Nucleic Acids Res **47**(22): 11574-11588.
Hollin, T., M. Gupta, T. Lenz and K. G. Le Roch (2021). "Dynamic Chromatin Structure and Epigenetics Control the Fate of Malaria Parasites." Trends Genet **37**(1): 73-85.
Iyer, L. M., S. Abhiman and L. Aravind (2008). "MutL homologs in restriction-modification systems and the origin of eukaryotic MORC ATPases." Biol Direct **3**: 8.
Iyer, L. M., V. Anantharaman, M. Y. Wolf and L. Aravind (2008). "Comparative genomics of transcription factors and chromatin proteins in parasitic protists and other eukaryotes." Int J Parasitol **38**(1): 1-31.
Jeninga, M. D., J. E. Quinn and M. Petter (2019). "ApiAP2 Transcription Factors in Apicomplexan Parasites." Pathogens **8**(2).
Jiang, L., J. Mu, Q. Zhang, T. Ni, P. Srinivasan, K. Rayavara, W. Yang, L. Turner, T. Lavstsen, T. G. Theander, W. Peng, G. Wei, Q. Jing, Y. Wakabayashi, A. Bansal, Y. Luo, J. M. Ribeiro, A. Scherf, L. Aravind, J. Zhu, K. Zhao and L. H. Miller (2013). "PfSETvs methylation of histone H3K36 represses virulence genes in Plasmodium falciparum." Nature **499**(7457): 223-227.
Josling, G. A., T. J. Russell, J. Venezia, L. Orchard, R. van Biljon, H. J. Painter and M. Llinas (2020). "Dissecting the role of PfAP2-G in malaria gametocytogenesis." Nat Commun **11**(1): 1503.
Kafsack, B. F., N. Rovira-Graells, T. G. Clark, C. Bancells, V. M. Crowley, S. G. Campino, A. E. Williams, L. G. Drought, D. P. Kwiatkowski, D. A. Baker, A. Cortes and M. Llinas (2014). "A transcriptional switch underlies commitment to sexual development in malaria parasites." Nature **507**(7491): 248-252.
Kang, H. G., W. C. Hyong, S. von Einem, P. Manosalva, K. Ehlers, P. P. Liu, S. V. Buxa, M. Moreau, H. G. Mang, P. Kachroo, K. H. Kogel and D. F. Klessig (2012). "CRT1 is a nuclear-translocated MORC endonuclease that participates in multiple levels of plant immunity." Nat Commun **3**: 1297.

749 Karmodiya, K., S. J. Pradhan, B. Joshi, R. Jangid, P. C. Reddy and S. Galande (2015). "A comprehensive
750 epigenome map of Plasmodium falciparum reveals unique mechanisms of transcriptional regulation
751 and identifies H3K36me2 as a global mark of gene suppression." Epigenetics Chromatin **8**: 32.
752 Kim, H., L. Yen, S. P. Wongpalee, J. A. Kirshner, N. Mehta, Y. Xue, J. B. Johnston, A. L. Burlingame, J. K.
753 Kim, J. J. Loparo and S. E. Jacobsen (2019). "The Gene-Silencing Protein MORC-1 Topologically Entraps
754 DNA and Forms Multimeric Assemblies to Cause DNA Compaction." Mol Cell **75**(4): 700-710 e706.
755 Koch, A., H. G. Kang, J. Steinbrenner, D. A. Dempsey, D. F. Klessig and K. H. Kogel (2017). "MORC
756 Proteins: Novel Players in Plant and Animal Health." Front Plant Sci **8**: 1720.
757 Lambros, C. and J. P. Vanderberg (1979). "Synchronization of Plasmodium falciparum erythrocytic
758 stages in culture." J Parasitol **65**(3): 418-420.
759 Le Roch, K. G., Y. Zhou, P. L. Blair, M. Grainger, J. K. Moch, J. D. Haynes, P. De La Vega, A. A. Holder, S.
760 Batalov, D. J. Carucci and E. A. Winzeler (2003). "Discovery of gene function by expression profiling of
761 the malaria parasite life cycle." Science **301**(5639): 1503-1508.
762 Love, M. I., W. Huber and S. Anders (2014). "Moderated estimation of fold change and dispersion for
763 RNA-seq data with DESeq2." Genome Biol **15**(12): 550.
764 Miao, J., C. Wang, A. B. Lucky, X. Liang, H. Min, S. R. Adapa, R. Jiang, K. Kim and L. Cui (2021). "A unique
765 GCN5 histone acetyltransferase complex controls erythrocyte invasion and virulence in the malaria
766 parasite Plasmodium falciparum." PLoS Pathog **17**(8): e1009351.
767 Modrzynska, K., C. Pfander, L. Chappell, L. Yu, C. Suarez, K. Dundas, A. R. Gomes, D. Goulding, J. C.
768 Rayner, J. Choudhary and O. Billker (2017). "A Knockout Screen of ApiAP2 Genes Reveals Networks of
769 Interacting Transcriptional Regulators Controlling the Plasmodium Life Cycle." Cell Host Microbe **21**(1):
770 11-22.
771 Moissiard, G., S. J. Cokus, J. Cary, S. Feng, A. C. Billi, H. Stroud, D. Husmann, Y. Zhan, B. R. Lajoie, R. P.
772 McCord, C. J. Hale, W. Feng, S. D. Michaels, A. R. Frand, M. Pellegrini, J. Dekker, J. K. Kim and S. E.
773 Jacobsen (2012). "MORC family ATPases required for heterochromatin condensation and gene
774 silencing." Science **336**(6087): 1448-1451.
775 Painter, H. J., T. L. Campbell and M. Llinas (2011). "The Apicomplexan AP2 family: integral factors
776 regulating Plasmodium development." Mol Biochem Parasitol **176**(1): 1-7.
777 Patro, R., G. Duggal, M. I. Love, R. A. Irizarry and C. Kingsford (2017). "Salmon provides fast and bias-
778 aware quantification of transcript expression." Nat Methods **14**(4): 417-419.
779 Perez-Riverol, Y., J. Bai, C. Bandla, D. Garcia-Seisdedos, S. Hewapathirana, S. Kamatchinathan, D. J.
780 Kundu, A. Prakash, A. Frericks-Zipper, M. Eisenacher, M. Walzer, S. Wang, A. Brazma and J. A. Vizcaino
781 (2022). "The PRIDE database resources in 2022: a hub for mass spectrometry-based proteomics
782 evidences." Nucleic Acids Res **50**(D1): D543-D552.
783 Pradhan, A., V. S. Chauhan and R. Tuteja (2005). "Plasmodium falciparum DNA helicase 60 is a schizont
784 stage specific, bipolar and dual helicase stimulated by PKC phosphorylation." Mol Biochem Parasitol
785 **144**(2): 133-141.
786 Quinn, J. E., M. D. Jeninga, K. Limm, K. Pareek, T. Meissgeier, A. Bachmann, M. F. Duffy and M. Petter
787 (2022). "The Putative Bromodomain Protein PfBDP7 of the Human Malaria Parasite Plasmodium
788 Falciparum Cooperates With PfBDP1 in the Silencing of Variant Surface Antigen Expression." Front Cell
789 Dev Biol **10**: 816558.
790 Real, E., F. Nardella, A. Scherf and L. Mancio-Silva (2022). "Repurposing of Plasmodium falciparum var
791 genes beyond the blood stage." Curr Opin Microbiol **70**: 102207.
792 Russell, T. J., E. K. De Silva, V. M. Crowley, K. Shaw-Saliba, N. Dube, G. Josling, C. F. A. Pasaje, I.
793 Kouskoumvekaki, G. Panagiotou, J. C. Niles, M. Jacobs-Lorena, C. Denise Okafor, F. J. Gamo and M.
794 Llinas (2022). "Inhibitors of ApiAP2 protein DNA binding exhibit multistage activity against Plasmodium
795 parasites." PLoS Pathog **18**(10): e1010887.
796 Santos, J. M., G. Josling, P. Ross, P. Joshi, L. Orchard, T. Campbell, A. Schieler, I. M. Cristea and M. Llinas
797 (2017). "Red Blood Cell Invasion by the Malaria Parasite Is Coordinated by the PfAP2-I Transcription
798 Factor." Cell Host Microbe **21**(6): 731-741 e710.

Sargeant, T. J., M. Marti, E. Caler, J. M. Carlton, K. Simpson, T. P. Speed and A. F. Cowman (2006). "Lineage-specific expansion of proteins exported to erythrocytes in malaria parasites." Genome Biol **7**(2): R12.

Scherf, A., R. Hernandez-Rivas, P. Buffet, E. Bottius, C. Benatar, B. Pouvelle, J. Gysin and M. Lanzer (1998). "Antigenic variation in malaria: in situ switching, relaxed and mutually exclusive transcription of var genes during intra-erythrocytic development in Plasmodium falciparum." EMBO J **17**(18): 5418-5426.

Scherf, A., J. J. Lopez-Rubio and L. Riviere (2008). "Antigenic variation in Plasmodium falciparum." Annu Rev Microbiol **62**: 445-470.

Schneider, V. M., J. E. Visone, C. T. Harris, F. Florini, E. Hadjimichael, X. Zhang, M. R. Gross, K. Y. Rhee, C. Ben Mamoun, B. F. C. Kafsack and K. W. Deitsch (2023). "The human malaria parasite Plasmodium falciparum can sense environmental changes and respond by antigenic switching." Proc Natl Acad Sci U S A **120**(17): e2302152120.

Shang, X., S. Shen, J. Tang, X. He, Y. Zhao, C. Wang, X. He, G. Guo, M. Liu, L. Wang, Q. Zhu, G. Yang, C. Jiang, M. Zhang, X. Yu, J. Han, R. Culleton, L. Jiang, J. Cao, L. Gu and Q. Zhang (2021). "A cascade of transcriptional repression determines sexual commitment and development in Plasmodium falciparum." Nucleic Acids Res **49**(16): 9264-9279.

Shang, X., C. Wang, Y. Fan, G. Guo, F. Wang, Y. Zhao, F. Sheng, J. Tang, X. He, X. Yu, M. Zhang, G. Zhu, S. Yin, J. Mu, R. Culleton, J. Cao, M. Jiang and Q. Zhang (2022). "Genome-wide landscape of ApiAP2 transcription factors reveals a heterochromatin-associated regulatory network during Plasmodium falciparum blood-stage development." Nucleic Acids Res **50**(6): 3413-3431.

Shang, X., C. Wang, L. Shen, F. Sheng, X. He, F. Wang, Y. Fan, X. He and M. Jiang (2021). "PfAP2-EXP2, an Essential Transcription Factor for the Intraerythrocytic Development of Plasmodium falciparum." Front Cell Dev Biol **9**: 782293.

Sierra-Miranda, M., S. S. Vembar, D. M. Delgadillo, P. A. Avila-Lopez, A. M. Herrera-Solorio, D. Lozano Amado, M. Vargas and R. Hernandez-Rivas (2017). "PfAP2Tel, harbouring a non-canonical DNA-binding AP2 domain, binds to Plasmodium falciparum telomeres." Cell Microbiol **19**(9).

Singh, M. K., G. Tessarin-Almeida, B. K. M. Dias, P. S. Pereira, F. Costa, J. M. Przyborski and C. R. S. Garcia (2021). "A nuclear protein, PfMORC confers melatonin dependent synchrony of the human malaria parasite P. falciparum in the asexual stage." Sci Rep **11**(1): 2057.

Singh, S., M. M. Alam, I. Pal-Bhowmick, J. A. Brzostowski and C. E. Chitnis (2010). "Distinct external signals trigger sequential release of apical organelles during erythrocyte invasion by malaria parasites." PLoS Pathog **6**(2): e1000746.

Singh, S., J. M. Santos, L. M. Orchard, N. Yamada, R. van Biljon, H. J. Painter, S. Mahony and M. Llinas (2021). "The PfAP2-G2 transcription factor is a critical regulator of gametocyte maturation." Mol Microbiol **115**(5): 1005-1024.

Sinha, A., K. R. Hughes, K. K. Modrzynska, T. D. Otto, C. Pfander, N. J. Dickens, A. A. Religa, E. Bushell, A. L. Graham, R. Cameron, B. F. C. Kafsack, A. E. Williams, M. Llinas, M. Berriman, O. Billker and A. P. Waters (2014). "A cascade of DNA-binding proteins for sexual commitment and development in Plasmodium." Nature **507**(7491): 253-257.

Smith, L. M., F. C. Motta, G. Chopra, J. K. Moch, R. R. Nerem, B. Cummins, K. E. Roche, C. M. Kelliher, A. R. Leman, J. Harer, T. Gedeon, N. C. Waters and S. B. Haase (2020). "An intrinsic oscillator drives the blood stage cycle of the malaria parasite Plasmodium falciparum." Science **368**(6492): 754-759.

Soneson, C., M. I. Love and M. D. Robinson (2015). "Differential analyses for RNA-seq: transcript-level estimates improve gene-level inferences." F1000Res **4**: 1521.

Srinivasan, P., A. Yasgar, D. K. Luci, W. L. Beatty, X. Hu, J. Andersen, D. L. Narum, J. K. Moch, H. Sun, J. D. Haynes, D. J. Maloney, A. Jadhav, A. Simeonov and L. H. Miller (2013). "Disrupting malaria parasite AMA1-RON2 interaction with a small molecule prevents erythrocyte invasion." Nat Commun **4**: 2261.

Srivastava, S., M. J. Holmes, M. W. White and W. J. Sullivan, Jr. (2023). "Toxoplasma gondii AP2XII-2 Contributes to Transcriptional Repression for Sexual Commitment." mSphere **8**(2): e0060622.

849 Strahl, B. D., P. A. Grant, S. D. Briggs, Z. W. Sun, J. R. Bone, J. A. Caldwell, S. Mollah, R. G. Cook, J.
850 Shabanowitz, D. F. Hunt and C. D. Allis (2002). "Set2 is a nucleosomal histone H3-selective
851 methyltransferase that mediates transcriptional repression." Mol Cell Biol **22**(5): 1298-1306.
852 Subudhi, A. K., J. L. Green, R. Satyam, T. Lenz, R. P. Salunke, M. Shuaib, I. Isaioglou, S. Abel, M. Gupta,
853 L. Esau, T. Mourier, R. Nugmanova, S. Mfarrej, R. Sivapurkar, Z. Stead, F. B. Rached, Y. Otswal, R.
854 Sougrat, A. Dada, A. F. Kadamany, W. Fischle, J. Merzaban, E. Knuepfer, D. J. P. Ferguson, I. Gupta, K.
855 G. L. Roch, A. A. Holder and A. Pain (2023). "PfAP2-MRP DNA-binding protein is a master regulator of
856 parasite pathogenesis during malaria parasite blood stages." bioRxiv: 2023.2005.2023.541898.
857 Subudhi, A. K., A. J. O'Donnell, A. Ramaprasad, H. M. Abkallo, A. Kaushik, H. R. Ansari, A. M. Abdel-
858 Haleem, F. Ben Rached, O. Kaneko, R. Culleton, S. E. Reece and A. Pain (2020). "Malaria parasites
859 regulate intra-erythrocytic development duration via serpentine receptor 10 to coordinate with host
860 rhythms." Nat Commun **11**(1): 2763.
861 Toenhake, C. G., S. A. Fraschka, M. S. Vijayabaskar, D. R. Westhead, S. J. van Heeringen and R. Bartfai
862 (2018). "Chromatin Accessibility-Based Characterization of the Gene Regulatory Network Underlying
863 Plasmodium falciparum Blood-Stage Development." Cell Host Microbe **23**(4): 557-569 e559.
864 Trager, W. and J. B. Jensen (1976). "Human malaria parasites in continuous culture." Science
865 **193**(4254): 673-675.
866 Wagner, E. J. and P. B. Carpenter (2012). "Understanding the language of Lys36 methylation at histone
867 H3." Nat Rev Mol Cell Biol **13**(2): 115-126.
868 Ward, P., L. Equinet, J. Packer and C. Doerig (2004). "Protein kinases of the human malaria parasite
869 Plasmodium falciparum: the kinome of a divergent eukaryote." BMC Genomics **5**: 79.
870 Yeoh, S., R. A. O'Donnell, K. Koussis, A. R. Dluzewski, K. H. Ansell, S. A. Osborne, F. Hackett, C. Withers-
871 Martinez, G. H. Mitchell, L. H. Bannister, J. S. Bryans, C. A. Kettleborough and M. J. Blackman (2007).
872 "Subcellular discharge of a serine protease mediates release of invasive malaria parasites from host
873 erythrocytes." Cell **131**(6): 1072-1083.
874 Yuda, M., S. Iwanaga, S. Shigenobu, G. R. Mair, C. J. Janse, A. P. Waters, T. Kato and I. Kaneko (2009).
875 "Identification of a transcription factor in the mosquito-invasive stage of malaria parasites." Mol
876 Microbiol **71**(6): 1402-1414.
877 Yuda, M., I. Kaneko, Y. Murata, S. Iwanaga and T. Nishi (2023). "Targetome Analysis of Malaria
878 Sporozoite Transcription Factor AP2-Sp Reveals Its Role as a Master Regulator." mBio **14**(1): e0251622.
879 Zhang, M., C. Wang, T. D. Otto, J. Oberstaller, X. Liao, S. R. Adapa, K. Udenze, I. F. Bronner, D. Casandra,
880 M. Mayho, J. Brown, S. Li, J. Swanson, J. C. Rayner, R. H. Y. Jiang and J. H. Adams (2018). "Uncovering
881 the essential genes of the human malaria parasite Plasmodium falciparum by saturation mutagenesis."
882 Science **360**(6388).
883 Zhang, Y., B. Bertulat, A. H. Tencer, X. Ren, G. M. Wright, J. Black, M. C. Cardoso and T. G. Kutateladze
884 (2019). "MORC3 Forms Nuclear Condensates through Phase Separation." iScience **17**: 182-189.
885 Zhong, Z., Y. Xue, C. J. Harris, M. Wang, Z. Li, Y. Ke, M. Liu, J. Zhou, Y. Jami-Alahmadi, S. Feng, J. A.
886 Wohlschlegel and S. E. Jacobsen (2023). "MORC proteins regulate transcription factor binding by
887 mediating chromatin compaction in active chromatin regions." Genome Biol **24**(1): 96.
888

889

890 **Figures Legends –**

891

892 **Figure 1 – Proteomic analysis of parasites expressing *Pf*MORC^{GFP} reveals *Pf*MORC**
893 **association with nuclear proteins of epigenetic regulation. (A)** Volcano plot illustrates the
894 protein enrichment in lable free LC-MS/MS analysis of *Pf*MORC CoIPed proteins from three
895 independent experiments at 32hpi. For normalized MS/MS counts, student's t-test was
896 performed and proteins were ranked as -log2 fold-change (x-axis) versus statistical *p-values* (y-
897 axis). Gray dashed horizontal line shows the *p-value* cutoff. **(B)** Comparative analysis showing
898 the juxtaposition of specific proteins CoIPed in PfMORC^{GFP} with selected proteins from recent
899 works of Hillier *et al.*, Bryant *et al.* and Subudhi *et al.* where ApiAP2 or ISW1 were used as
900 bait in similar CoIP experiments. The Venn diagram illustrates the overlap between identified
901 proteins, revealing that the intersecting proteins are primarily ApiAP2 and chromatin
902 remodellers. **(C)** An interactive protein-protein interaction network is constructed with proteins
903 known to interact with PfMORC, using proteins identified in this study and proteins
904 documented in previously published works. Proteins identified in this study with known
905 interaction networks from the STRING database were used to curate the network employing
906 Cytoscape to enrich the network quality.

907

908 **Figure 2 – Genome-wide occupancy of *Pf*MORC reveals localization to hypervariable**
909 **surface antigen genes at 30 h and 40 h. (A)** Coverage tracks of *Pf*MORC across all 14 *P.*
910 *falciparum* chromosomes. Plotted values are fold enrichment (Log2[IP/Input]) of a
911 representative replicate at 30 h. **(B)** Zoom-in of the last 100kb region of chromosome two from
912 Panel A. Gene annotations represented in blue bars (*P. falciparum* 3D7 strain, version 3, release
913 57; PlasmoDB.org). **(C)** Mean fold enrichment of *Pf*MORC occupancy across all var genes (top
914 left), all rif genes (top right), and all stevor genes (bottom right), excluding pseudogenes.
915 Graphical representation of exons to scale for each gene family annotated below enrichment
916 plot in grey (e1=exon one; e2=exon two). **(D)** Quantitative Venn diagram comparing the
917 number of MACS2 called peaks across each timepoint (light pink for 30 h; dark pink for 40 h).
918 **(E)** Pie charts showing the type of genomic locations *Pf*MORC peaks overlap at both 30 h and
919 40 h. Pink slices are 5` regions upstream of the ATG start site of genes, blue slices are coding
920 sequences/gene bodies of genes, and green slices are 3` regions downstream of the stop codon
921 of genes. **(F)** Zoom-in of the first 100kb region (left) and the last 100kb region (right) of
922 chromosome two. Plotted are the ChIP-seq fold enrichment of *Pf*MORC (top track; pink) and
923 heterochromatin protein 1 (HP1; middle track; orange) with gene annotations (bottom track;
924 blue bars; *P. falciparum* 3D7 strain, version 3, release 57; PlasmoDB.org).

925

926 **Figure 3** – **(A)** Mean fold enrichment (Log2[IP/Input]) of *Pf*MORC, six associated factors
927 (AP2-G5, AP2-O5, AP2-I, PF3D7_1107800, PF3D7_0613800, and PF3D7_1239200), HP1,
928 and a negative no-epitope control across *Pf*MORC binding sites at the 30 h timepoint. **(B)** Mean
929 fold enrichment (Log2[IP/Input]) of *Pf*MORC, six associated factors (AP2-G5, AP2-O5, AP2-
930 I, PF3D7_1107800, PF3D7_0613800, and PF3D7_1239200), HP1, and a negative no-epitope
931 control across *Pf*MORC binding sites at the 40 h timepoint. **(C)** Mean fold enrichment
932 (Log2[IP/Input]) and heatmap of two H3K36me2 epigenetic mark timepoints across *Pf*MORC
933 binding sites at 30 h. **(D)** Mean fold enrichment (Log2[IP/Input]) and heatmap of two
934 H3K36me2 epigenetic mark timepoints across *Pf*MORC binding sites at 40 h.

935

936 **Figure 4 – Transcriptome analysis of *Pf*MORC knockdown revealed differential gene**
937 **expression.** (**A**) Volcano plot displaying the differential gene expression in *Pf*MORC-KD
938 compared to the *Pf*MORC-WT phenotype. Tightly synchronized PfMORC$^{HA\text{-}glmS}$ parasites (32
939 hpi ± 3 h) were split into two populations, one of which was treated with 2.5 mM GlcN to
940 obtain the *Pf*MORC knockdown phenotype and the other was not treated with GlcN to obtain
941 wild-type phenotype. Total RNA-seq was performed, and significant threshold parameters for
942 DEGs were assigned to a *p-value* < 0.05 and -log2 fold change > 1 from three biological
943 replicates. **(B)** Scatter plot shows upregulated and downregulated DEGs which were further
944 categorized for pathway and functional enrichment analysis using the KEGG database (p-
945 adjusted value < 0.05). The circle size at the vertical axis represents the number of genes in the
946 enriched pathways and the horizontal axis represents gene richness as a ratio of DEGs in the
947 pathways to the total genes in a specific pathway. **(C)** The violin plot of $\log_2$ fold change of
948 genes belonging to the multigene family is constructed from *Pf*MORC-KD vs *Pf*MORC-WT,
949 which shows DEGs of multigene family proteins upon *Pf*MORC knockdown. **(D)** The bar plot
950 illustrates the upregulated DEGs of apical organelle origin in *Pf*MORC-KD parasites involved
951 in host cell invasion. **(E)** Venn diagram showing the comparison between genes obtained from
952 ChIP-seq data and DEGs obtained from RNA-seq data. Both 30hpi and 40 hpi time points were
953 taken for comparison and showed high overlap with each other but there was no overlap with
954 RNA-seq data.

955

956

957

958 **Supplemental Figures**

959

960 **Supplemental Figure 1 –**

961 **(A)** Coomassie-stained 6% SDS–PAGE gel showing the parasite lysate of wild-type 3D7 and
962 *Pf*MORC^{GFP} after coimmunoprecipitation with anti-GFP magnetic beads. Both lanes were used
963 for mass spectrometry analysis. **(B)** Histogram shows the total proteins identified in mass
964 spectrometry analysis from three biological replicates in wild-type 3D7 and *Pf*MORC^{GFP}
965 coimmunoprecipitated samples. Venn diagram illustrates the labeled free LC-MS/MS
966 enrichment of peptide hits obtained from **(C)** 3D7 control and **(D)** from *Pf*MORC^{GFP} parasites
967 lysate. Briefly, 32 hpi (±4 h) trophozoite stage parasites were harvested and lysed, followed by
968 incubation with anti-GFP-Trap-A beads from three independent biological replicates were used
969 for quantification. False discovery rate (FDR) of 1% and peptides ≥2 leads to identifying 191,
970 814, 589 and 211, 617, 656 significant proteins in 3D7 and *Pf*MORC^{GFP}, respectively. **(E)**
971 MS/MS normalization of identified proteins from 3D7 parasites expressing *Pf*MORC and
972 transgenic parasites expressing GFP (*Pf*MORC^{GFP}) was carried out. Gene ontology
973 classification showing biological process, cellular component, and molecular function of
974 *Pf*MORC^{GFP}/3D7 normalized proteins showing fold change ≥ 1.5.

975

976 **Supplemental Figure 2 –**

977 **(A)** Correlation plot (DeepTools PlotCorrelation) of the 30 h samples compared to the negative
978 control ChIP-seq sample. **(B)** Correlation plot (DeepTools PlotCorrelation) of the 40 h samples
979 compared to the negative control ChIP-seq sample. **(C)** Violin plot showing the ChIP-seq fold
980 enrichment values of significantly called peaks in all 6 biological replicates. The two GFP
981 samples were only used as additional controls for comparison purposes. **(D)** Venn diagram
982 comparing the overlap of MACS2-called peaks between anti-HA biological replicates at 30 h.
983 **(E)** Venn diagram comparing the overlap of MACS2-called peaks between anti-HA biological
984 replicates at 40 h. (F) Venn diagram comparing the overlap of MACS2-called peaks between
985 anti-GFP biological replicates at 40 h.

986

987 **Supplemental Figure 3 –**

988 **(Top)** Profile plot of the mean *Pf*MORC ChIP-seq fold enrichment (Log2[IP/Input]) for all four
989 samples across all PfEMP1 (var) gene 5` upstream regions and gene bodies. **(Bottom)** Heatmap
990 of the *Pf*MORC ChIP-seq fold enrichment (Log2[IP/Input]) for all four samples across all
991 *Pf*EMP1 (*var*) gene 5` upstream regions and gene bodies. **(Inset to the right)** Zoom in on the
992 average enrichment of *Pf*MORC at var genes with annotated exons.

993

994 **Supplemental Figure 4 –**

995 **(Top)** Profile plot of the mean *Pf*MORC ChIP-seq fold enrichment (Log2[IP/Input]) for all four
996 samples across all *rif* gene 5` upstream regions and gene bodies. **(Bottom)** Heatmap of the
997 *Pf*MORC ChIP-seq fold enrichment (Log2[IP/Input]) for all four samples across all *rif* gene 5`
998 upstream regions and gene bodies. **(Inset to the right)** Zoom in on the average enrichment of
999 *Pf*MORC at *rif* genes with annotated exons.

1000

1001

1002 **Supplemental Figure 5 –**

1003 **(Top)** Profile plot of the mean *Pf*MORC ChIP-seq fold enrichment (Log2[IP/Input]) for all four
1004 samples across all *rif* gene 5` upstream regions and gene bodies. **(Bottom)** Heatmap of the
1005 *Pf*MORC ChIP-seq fold enrichment (Log2[IP/Input]) for all four samples across all *rif* gene 5`
1006 upstream regions and gene bodies. **(Inset to the right)** Zoom in on the average enrichment of
1007 *Pf*MORC at *rif* genes with annotated exons.

1008

1009 **Supplemental Figure 6 –**

1010 The heatmaps show the transcript abundance (Chappell et al. 2020) of putative *Pf*MORC gene
1011 targets at 30 h (left) and 40 h (right). Red signifies high transcript abundance, and green signifies
1012 low transcript abundance. Both timepoints are organized into two major clusters (highlighted
1013 with the yellow bar and blue bar).

1014

1015 **Supplemental Figure 7 –**

1016 **(A)** Associated with Figure 3A,B. Mean fold enrichment (Log2[IP/Input]) summary plot (top) and
1017 full heatmap (bottom) of fold enrichment of PfMORC, six associated ApiAP2 factors (AP2-
1018 G5, AP2-O5, AP2-I, PF3D7_1107800, PF3D7_0613800, and PF3D7_1239200), HP1, and a
1019 negative no-epitope control across *Pf*MORC binding sites at the 30 h and 40 h timepoints. **(B)**
1020 Quantitative Venn diagrams of the binding site overlaps between *Pf*MORC and the six associated
1021 ApiAP2 factors.

1022

1023 **Supplemental Figure 8 –**

1024 DNA motif analyses from these different categories: (1) Unique to 30 hpi ChIP-seq Timepoint,
1025 (2) 30hpi ChIP-seq Timepoint, (3) Overlap of ChIP-seq Timepoints, (4) 40hpi ChIP-seq
1026 Timepoint, and (5) Unique to 30hpi ChIP-seq Timepoint. The values to the right of each motif
1027 contain the enrichment value, number of peaks containing that motif, and percent of the peaks
1028 the contain that motif calculated by Meme Suite.

1029

1030 **Supplemental Figure 9 –**

1031 Mean fold enrichment (Log2[IP/Input]) summary plot (top) and full heatmap (bottom) of fold
1032 enrichment of ten selected epigenetic marks (H2A.Z, H3K9ac, H3K4me3, H3K27ac, H3K18ac,
1033 H3K9me3, H3K36me2/3, H4K20me3, and H3K4me1) across *Pf*MORC binding sites at the 30
1034 h and 40 h timepoints.

1035

1036 **Supplemental Figure 10 –**

1037 **Comparison of transcriptional changes with melatonin treatment. (A)** Volcano plot
1038 showing the differentially expressed genes in *Pf*MORC-KD parasites relative to *Pf*MORC-WT
1039 after 100 nM melatonin treatment for 5h from three independent experiments. **(B)** Venn

1040 diagram shows intersecting DEGs from the experiment with KD vs WT with DEGs obtained
1041 from the experiment (KD vs WT) treated with 100 nM melatonin for 5 h. Number of DEGs are
1042 shown as up (red) and downregulated (green). The intersecting region shows 282 upregulated
1043 and 340 downregulated genes. Heatmap showing significant DEGs based on *p-values* and
1044 $\log_2$FD for upregulating (**C**) and downregulating (**D**). These genes are taken from 622
1045 intersecting DEGs showing partial changes in expression after melatonin treatment.

1046

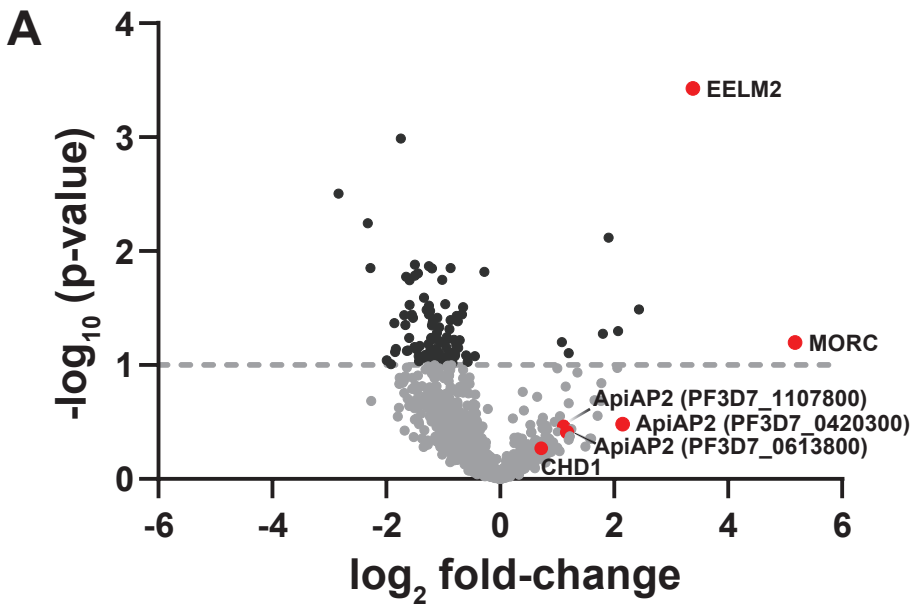
A
EELM2
MORC
ApiAP2 (PF3D7_1107800)
ApiAP2 (PF3D7_0420300)
ApiAP2 (PF3D7_0613800)
CHD1
-log10 (p-value)
log2 fold-change
4
3
2
1
0
-6
-4
-2
0
2
4
6

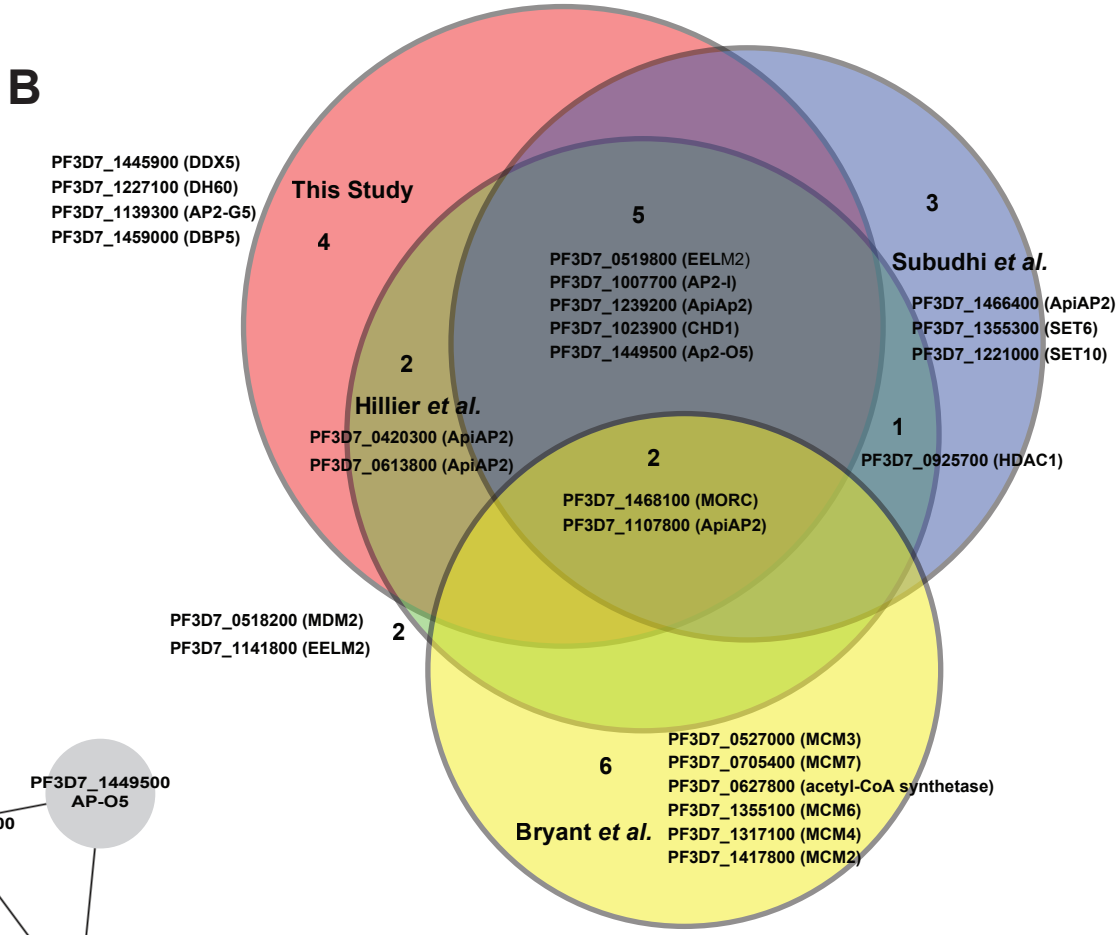
B
This Study
PF3D7_1445900 (DDX5)
PF3D7_1227100 (DH60)
PF3D7_1139300 (AP2-G5)
PF3D7_1459000 (DBP5)
4
5
PF3D7_0519800 (EELM2)
PF3D7_1007700 (AP2-I)
PF3D7_1239200 (ApiAp2)
PF3D7_1023900 (CHD1)
PF3D7_1449500 (Ap2-O5)
3
Subudhi et al.
PF3D7_1466400 (ApiAP2)
PF3D7_1355300 (SET6)
PF3D7_1221000 (SET10)
2
Hillier et al.
PF3D7_0420300 (ApiAP2)
PF3D7_0613800 (ApiAP2)
1
PF3D7_0925700 (HDAC1)
2
PF3D7_1468100 (MORC)
PF3D7_1107800 (ApiAP2)
PF3D7_0518200 (MDM2)
PF3D7_1141800 (EELM2)
2
6
PF3D7_0527000 (MCM3)
PF3D7_0705400 (MCM7)
PF3D7_0627800 (acetyl-CoA synthetase)
PF3D7_1355100 (MCM6)
PF3D7_1317100 (MCM4)
PF3D7_1417800 (MCM2)
Bryant et al.

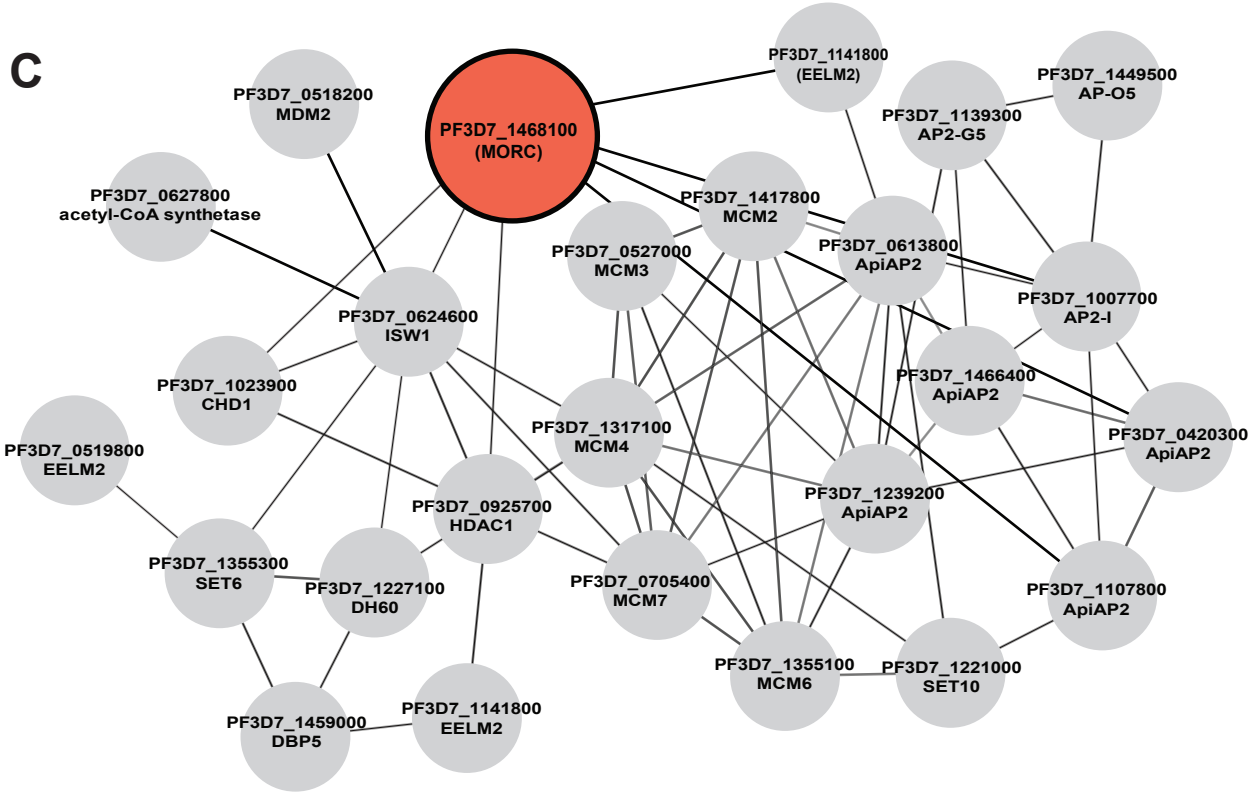
C
PF3D7_1468100 (MORC)
PF3D7_1141800 (EELM2)
PF3D7_1449500 AP-O5
PF3D7_1139300 AP2-G5
PF3D7_0518200 MDM2
PF3D7_0627800 acetyl-CoA synthetase
PF3D7_1417800 MCM2
PF3D7_0527000 MCM3
PF3D7_0613800 ApiAP2
PF3D7_1007700 AP2-I
PF3D7_0624600 ISW1
PF3D7_1466400 ApiAP2
PF3D7_1023900 CHD1
PF3D7_1317100 MCM4
PF3D7_0420300 ApiAP2
PF3D7_0519800 EELM2
PF3D7_1239200 ApiAP2
PF3D7_0925700 HDAC1
PF3D7_1355300 SET6
PF3D7_1227100 DH60
PF3D7_0705400 MCM7
PF3D7_1107800 ApiAP2
PF3D7_1355100 MCM6
PF3D7_1221000 SET10
PF3D7_1459000 DBP5
PF3D7_1141800 EELM2

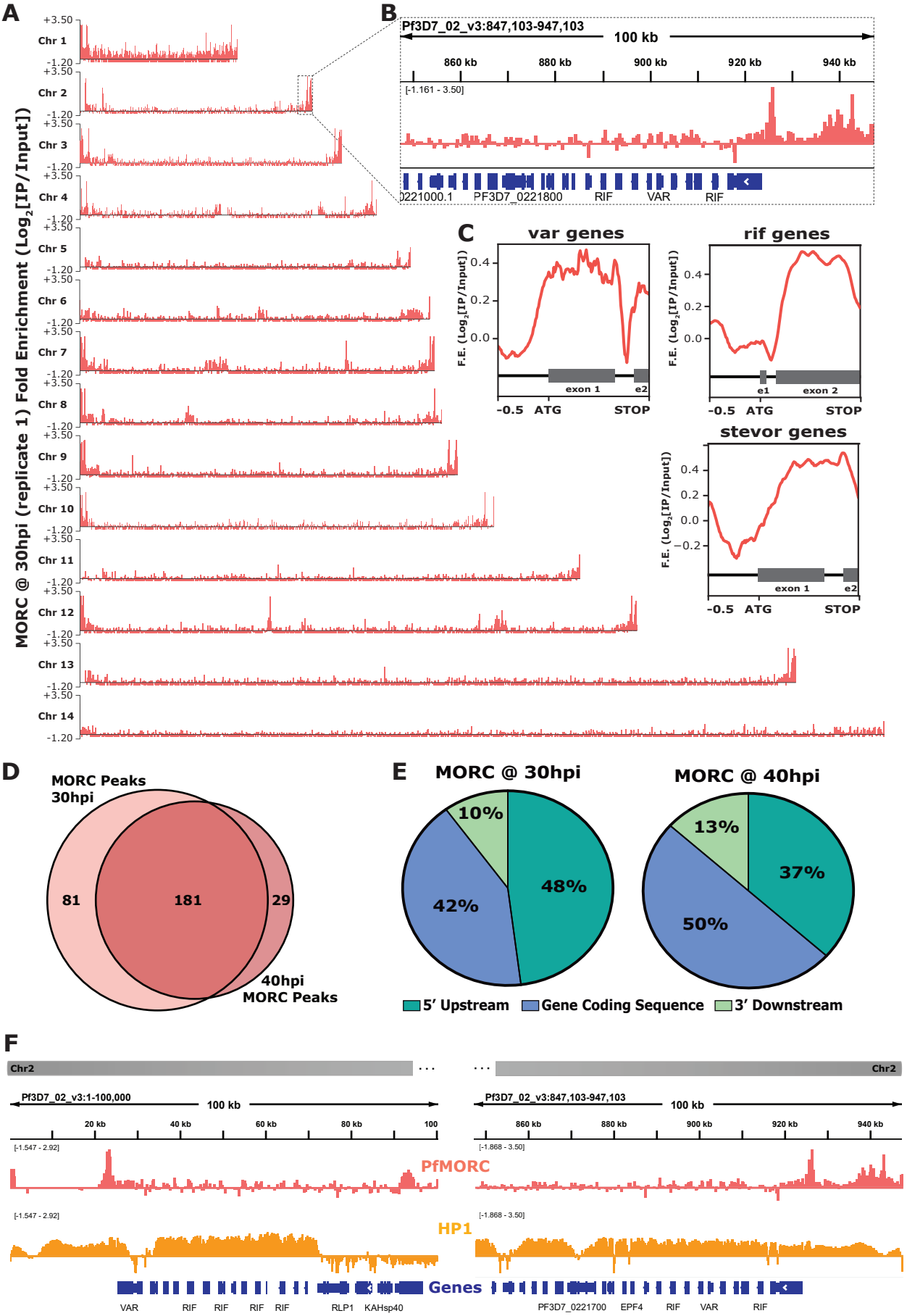
A
MORC @ 30hpi (replicate 1) Fold Enrichment (Log2[IP/Input])
+3.50
-1.20
Chr 1
Chr 2
Chr 3
Chr 4
Chr 5
Chr 6
Chr 7
Chr 8
Chr 9
Chr 10
Chr 11
Chr 12
Chr 13
Chr 14
B
Pf3D7_02_v3:847,103-947,103
100 kb
860 kb
880 kb
900 kb
920 kb
940 kb
[-1.161 - 3.50]
0221000.1
PF3D7_0221800
RIF
VAR
RIF
C
var genes
rif genes
stevor genes
F.E. (Log2[IP/Input])
exon 1
e2
e1
exon 2
-0.5
ATG
STOP
D
MORC Peaks
30hpi
81
181
29
40hpi
MORC Peaks
E
MORC @ 30hpi
10%
48%
42%
MORC @ 40hpi
13%
37%
50%
5′ Upstream
Gene Coding Sequence
3′ Downstream
F
Chr2
Pf3D7_02_v3:1-100,000
100 kb
20 kb
40 kb
60 kb
80 kb
100
[-1.547 - 2.92]
Pf3D7_02_v3:847,103-947,103
860 kb
880 kb
900 kb
920 kb
940 kb
[-1.868 - 3.50]
PfMORC
HP1
Genes
VAR
RIF
RIF
RIF
RIF
RLP1
KAHsp40
PF3D7_0221700
EPF4
RIF
VAR
RIF

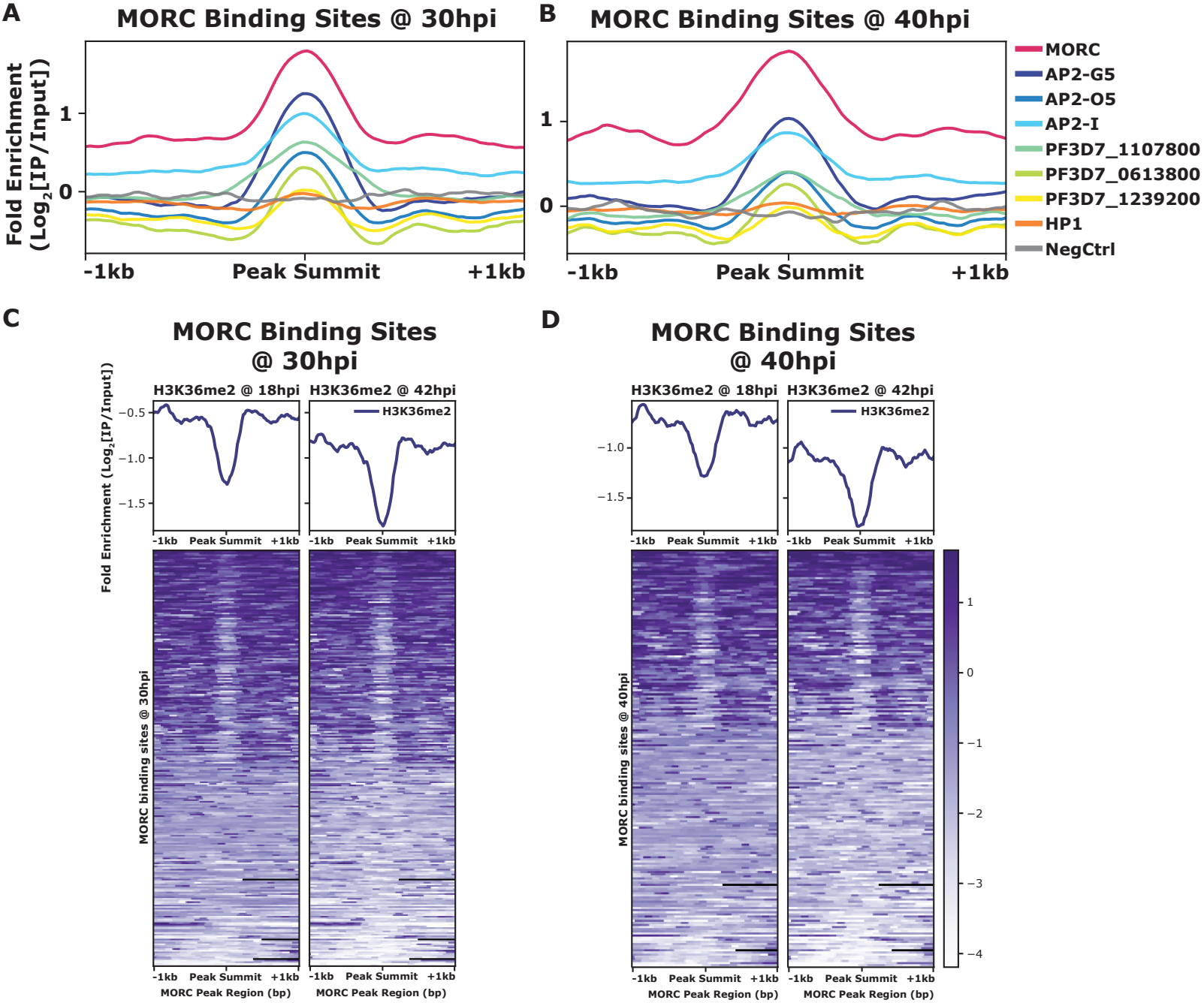
A
MORC Binding Sites @ 30hpi
Fold Enrichment (Log2[IP/Input])
1
0
-1kb
Peak Summit
+1kb
B
MORC Binding Sites @ 40hpi
1
0
-1kb
Peak Summit
+1kb
MORC
AP2-G5
AP2-O5
AP2-I
PF3D7_1107800
PF3D7_0613800
PF3D7_1239200
HP1
NegCtrl
C
MORC Binding Sites @ 30hpi
H3K36me2 @ 18hpi
H3K36me2 @ 42hpi
H3K36me2
Fold Enrichment (Log2[IP/Input])
−0.5
−1.0
−1.5
-1kb Peak Summit +1kb
MORC binding sites @ 30hpi
MORC Peak Region (bp)
D
MORC Binding Sites @ 40hpi
H3K36me2 @ 18hpi
H3K36me2 @ 42hpi
H3K36me2
−1.0
−1.5
-1kb Peak Summit +1kb
MORC binding sites @ 40hpi
MORC Peak Region (bp)
1
0
−1
−2
−3
−4

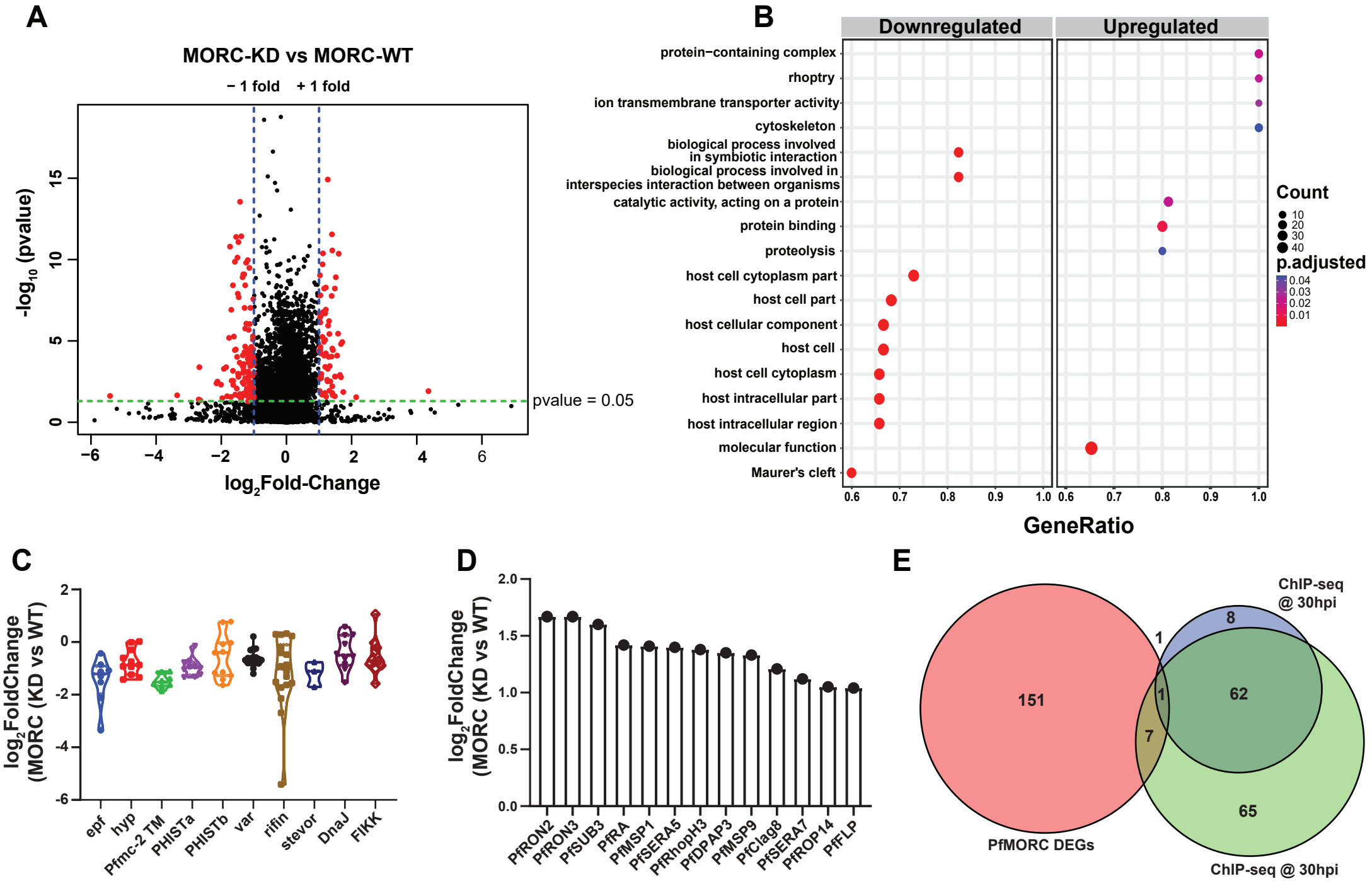
A
MORC-KD vs MORC-WT
− 1 fold
+ 1 fold
-log10 (pvalue)
log2Fold-Change
pvalue = 0.05
B
Downregulated
Upregulated
protein−containing complex
rhoptry
ion transmembrane transporter activity
cytoskeleton
biological process involved in symbiotic interaction
biological process involved in interspecies interaction between organisms
catalytic activity, acting on a protein
protein binding
proteolysis
host cell cytoplasm part
host cell part
host cellular component
host cell
host cell cytoplasm
host intracellular part
host intracellular region
molecular function
Maurer's cleft
GeneRatio
Count
p.adjusted
C
log2FoldChange (MORC (KD vs WT)
epf
hyp
Pfmc-2 TM
PHISTa
PHISTb
var
rifin
stevor
DnaJ
FIKK
D
log2FoldChange (MORC (KD vs WT)
PfRON2
PfRON3
PfSUB3
PfRA
PfMSP1
PfSERA5
PfRhopH3
PfDPAP3
PfMSP9
PfClag8
PfSERA7
PfROP14
PfFLP
E
ChIP-seq @ 30hpi
PfMORC DEGs
ChIP-seq @ 30hpi
151
1
8
1
62
7
65